Hindawi
Shock and Vibration
Volume 2022, Article ID 6399675, 30 pages
https://doi.org/10.1155/2022/6399675

*Research Article*

# Free Vibration Analysis of Cross-Ply Laminated Conical Shell, Cylindrical Shell, and Annular Plate with Variable Thickness Using the Haar Wavelet Discretization Method

**Jangsu Kim**,[1] **Kwanghun Kim**,[2] **Kwangil Kim**,[3] **Kwonryong Hong**,[4] **and Chonghyok Paek**[1]

[1]*Information Technology Center, High-Technology Development Institution, Kim Il Sung University, Pyongyang, Democratic People's Republic of Korea*
[2]*Department of Engineering Machine, Pyongyang University of Mechanical Engineering, Pyongyang 999093, Democratic People's Republic of Korea*
[3]*Department of Physics, Kim Il Sung University, Pyongyang, Democratic People's Republic of Korea*
[4]*Institute of Natural Sciences, Kim Il Sung University, Pyongyang, Democratic People's Republic of Korea*

Correspondence should be addressed to Jangsu Kim; kjs19821003@163.com and Kwanghun Kim; kimkwanghun@163.com

Received 5 July 2022; Revised 7 August 2022; Accepted 17 August 2022; Published 3 October 2022

Academic Editor: Vasudevan Rajamohan



This paper presents a unified solution method to investigate the free vibration behaviors of a laminated composite conical shell, a cylindrical shell, and an annular plate with variable thickness and arbitrary boundary conditions using the Haar wavelet discretization method (HWDM). Theoretical formulation is established based on the first-order shear deformation theory (FSDT), and displacement components are extended to the Haar wavelet series in the axis direction and trigonometric series in the circumferential direction. The constants generated by the integration process are disposed by boundary conditions, and thus the equations of the motion of the total system, including the boundary condition, are transformed into algebraic equations. Then, the natural frequencies of the laminated composite structures are directly obtained by solving these algebraic equations. The stability and accuracy of the present method are verified through convergence and validation studies. The effects of some material properties and geometric parameters on the free vibration of laminated composite shells are discussed and some related mode shapes are given. Some new results for laminated composite conical shell, cylindrical shell, and annular plate with variable thickness and arbitrary boundary conditions are presented, which may serve as benchmark solutions.

## 1. Introduction

Conical shell, cylindrical shell, and annular plate are widely used in a variety of engineering fields, such as mechanical, architectural, aerospace, marine, and other industries. With the development of science and manufacturing technology, various composite materials, such as laminated composite and functionally graded material have emerged, and many studies have been conducted on the dynamic characteristics of various shell structures made of these composite materials. Studies on structures, such as cylindrical shells [1–10], conical shells [8–20], and annular plates [8–10] with uniform thickness have been presented in many pieces of literature. However, the structures with variable thickness are present in the actual engineering applications, and it is needed to analyze their vibration characteristics accurately.

Based on the classical thin shell theory, Irie et al. [21] carried out the analysis on the free vibration of a truncated conical shell with variable thickness using the transfer matrix approach and calculated the natural frequencies and mode shapes numerically. Sivadas and Ganesan [22–26] investigated the asymmetric free vibration behavior of isotropic cantilever conical shell, circular cylindrical shell, and laminated cylindrical, conical shells with variable thickness using Love's first approximation thin shell theory and finite element method, and Gautham and Ganesan [27] analyzed the

axisymmetric free vibration if thick orthotropic spherical shells were with linearly varying thickness along the meridian. Sankaranarayanan et al. [28, 29] analyzed the free vibration of the laminated conical shells of variable thickness using the classical thin shell theory and energy method based on the Rayleigh-Ritz procedure. Jiang and Redekop [30] developed a solution method based on the Sanders-Budiansky shell equations for analyzing the static and free vibration characteristics of linear elastic orthotropic toroidal shells of variable thickness. In this study, the thickness of shell is changed in a circumferential direction. Duan and Koh [31] derived analytical solutions for the axisymmetric transverse vibration of cylindrical shells with variable thickness for the first time, in which solutions are derived in terms of generalized hypergeometric function. Based on the classical Donnell's theory, Chen et al. [32] performed the buckling analysis on the cylindrical shells with variable thickness using the perturbation technique, in which the variation of thickness is in the axial direction. Liu et al. [33] presented an analytical method based on the Flügge theory and an equivalent method of ring-stiffeners for the free vibration of a fluid loaded ring-stiffened conical shell with variable thickness in the low frequency range. Tran et al. [34] studied the vibration characteristics of functionally graded cylindrical shells with the variable thickness, in which the thickness of the shell varies linearly along the longitudinal direction, using the FSDT and Hamilton's principle. Nihal and David [35] formulated the dynamic stiffness equation for variable thickness cylindrical shells based on the Donnell, Timoshenko, and Flugge theories and obtained the natural frequencies using the Wittrick-Williams algorithm. Afonso and Hinton [36, 37] studied the free vibration characteristics of plates and shells with an arbitrary thickness variation and boundary conditions using the finite element method (FEM). Based on the classical Donnell's and Love's shell theories, Taati et al. [38] investigated the free vibration characteristics of thin cylindrical shells with variable thickness and a constant angular velocity. Efraim and Eisenberger [39] obtained the free vibration frequencies and mode shapes of thick spherical shell segments with variable thickness and different boundary conditions using the dynamic stiffness method. Zheng et al. [40] applied the energy method based on the Donnell-Mushtari shell theory to investigate the vibration characteristics of the cylindrical shell with arbitrary variable thickness and general boundary conditions. The references related to the vibration analysis of shells with variable thickness can be found in Tornabene's studies [41–46] and Kang's studies [47–54]. There are many pieces of literature on the free vibration analysis of shells and plates with variable thickness, however, the free vibration analysis of laminated composite structures with variable thickness is almost impossible to find. Therefore, the focus of this paper is on the free vibration analysis of the laminated composite conical shell, cylindrical shell, and annular plate with variable thickness. In the vibration analysis of structures, to select a reasonable solution method is very important to satisfy the accuracy and efficiency of calculation.

Recently, the Haar wavelets, first introduced by Alfred Haar in 1910, have attracted the considerable attention of researchers because it is mathematically the simplest orthogonal compactly supported wavelet of all wavelet families, and the solution procedure is simple and direct. The Haar wavelet method has been proven to be an effective tool for solving various problems, such as differential and integral equations, biharmonic equations, and Poisson equations [55–63]. In addition, the Haar wavelet has been also proven to be an effective tool for solving the static and dynamic problems of various structures, such as beams [64–68], plates [9, 69, 70], and shells [4–6, 9, 11, 71–75]. Therefore, in this paper, the Haar wavelet discretization method, whose effectiveness has been verified in the vibration analysis of various laminated composite shell structures, is selected to investigate the free vibration characteristics of laminated composite conical, cylindrical, and annular plate. The natural frequency obtained by this method is compared with that obtained in previous literature and FEM. The effects of some parameters on the free vibration of considered structures are discussed, and new results of the frequency parameters and mode shapes are given.

## 2. Theoretical Formulations

*2.1. Description of the Model.* The geometric relations and coordinate system of the laminated composite conical shell, cylindrical shell, and annular plate are shown in Figure 1. The reference surface is defined by the geometric middle surface.

The fiber orientation angle of the $k^{th}$ layer is represented by $\phi$f. The coordinate system $x$, $\theta$, $z$ of the laminated composite structures is introduced, and the displacements in the axial, circumferential, and normal directions are denoted by $u$, v, and $w$, respectively. To generalize of the boundary conditions, the elastic spring technique is introduced, and the linear elastic springs in the axial, circumferential, and normal directions are represented as ku, kv, and kw, and the rotation springs in the $\theta$- and $x$-axis direction are denoted as k$\varphi$ and k$\theta$, respectively. The cone length and cone semivertex angle of the conical shell are denoted by $L$ and $\varphi$, respectively. R1 and R2 are the small and large radius and the radius $R$ is a function of axial coordinate $x$. The semivertex angle $\varphi$ is denoted by the angle between the $x$-axis and the rotating axis. In Figure 1(c), it is worth noting that, by setting the semivertex angle $\varphi = 0$, we can reduce the formulation of conical shells to that of cylindrical shells. In addition, by setting the semivertex angle $\varphi = \pi/2$, we can reduce the formulation of conical shells to that of annular plate with outer radius R2 and inner radius R1.

The thicknesses at origin and end of the shell are represented by h1 and h2, respectively, and the generalized equation of thickness depends on the following:

$$h(x) = h_1\left[1 - \alpha\left(\frac{x}{L}\right)^{\lambda}\right], \tag{1}$$

where $\alpha$ and $\lambda$ are thickness variation parameters.

Figures 2 and 3 show the change curves of thickness profile according to the change of $\alpha$ and $\lambda$. In Figure 2, the thickness of structure in $\alpha = 0$ is uniform, and it is increased

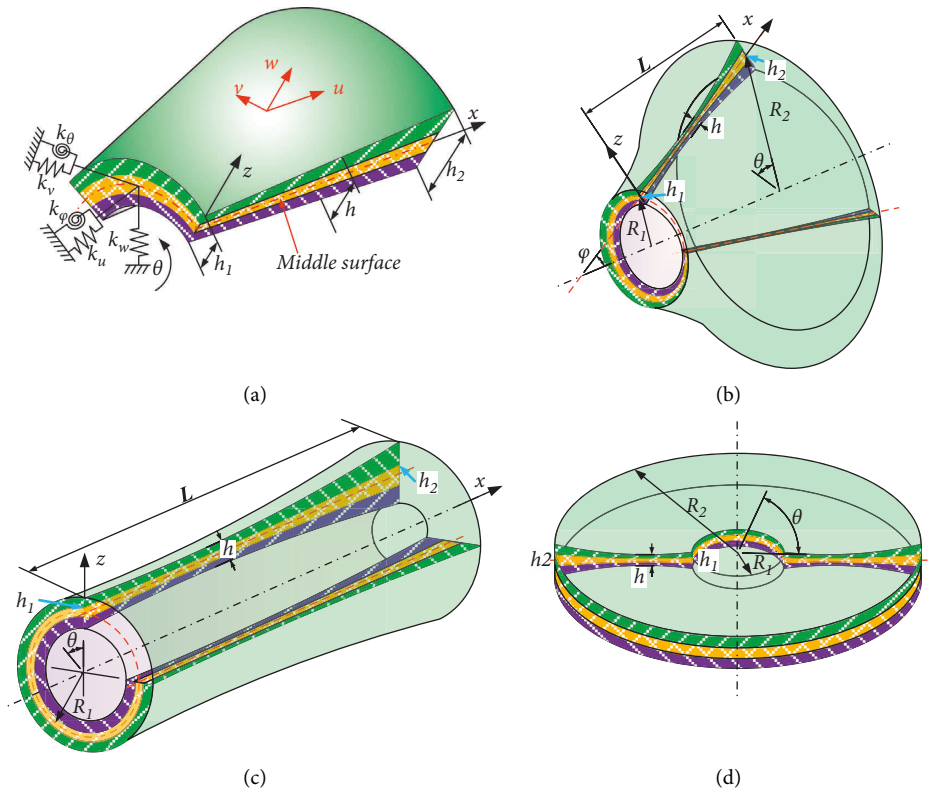


Figure 1: The diagram of the laminated composite structure with variable thickness, (a) cross-section view and boundary condition, (b) conical shell, (c) cylindrical shell, and (d) annular plate.

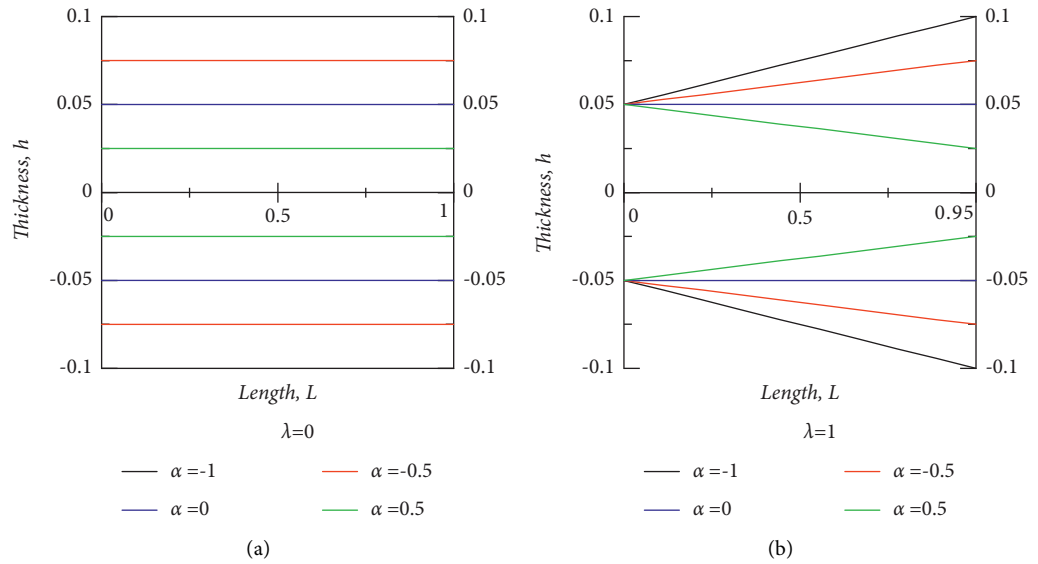


Figure 2: Change of thickness profile according to thickness variation parameter $\alpha$.

or decreased according to the changes of $\alpha$. Then, according to the changes of $\lambda$, the thickness profile is linearly or nonlinearly changed in Figure 3. Especially, when $\lambda = 1$, whatever $\alpha$ is, the thickness of structure is linearly increased or decreased.

*2.2. Formulation for Analysis.* In the present study, FSDT is employed for driving the equation of motion for the considered structures. According to FSDT, for any point within the shell, the displacement and rotation components of the reference plane can be written as follows [3, 7–9]:

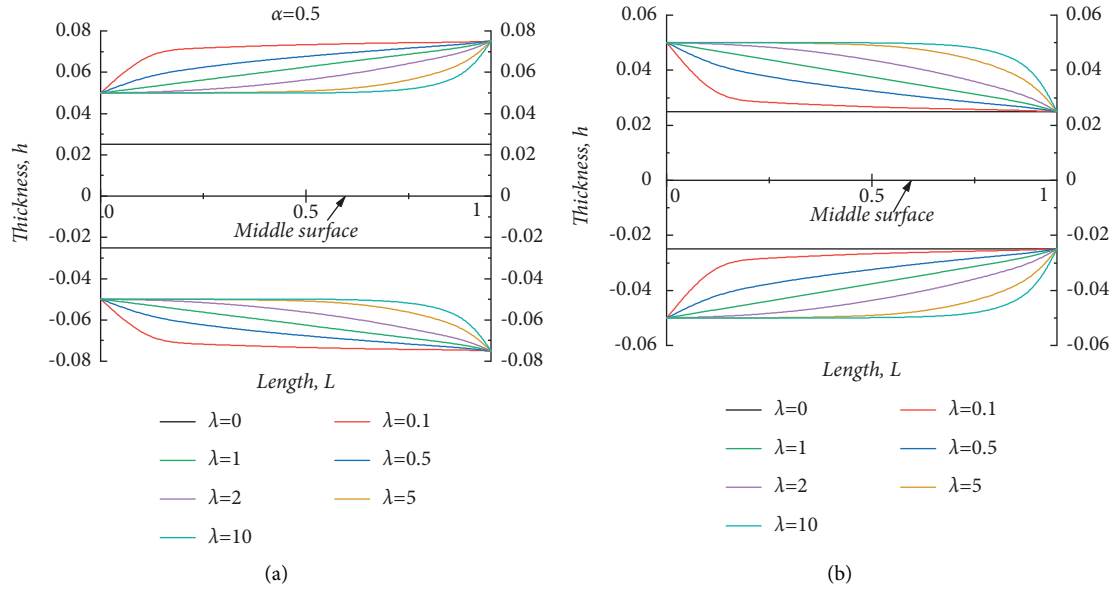


Figure 3: Change of thickness profile according to thickness variation parameter $\lambda$.

$$u(x,\theta,z,t) = u_0(x,\theta,t) + z\phi_x(x,\theta,t)$$
$$v(x,\theta,z,t) = v_0(x,\theta,t) + z\phi_\theta(x,\theta,t), \quad (2)$$
$$w(x,\theta,z,t) = w_0(x,\theta,t)$$

where u0, v0, and w0 are the displacements at a point of the middle surface, along axial, circumferential, and normal directions, respectively. $\phi$x and $\phi\theta$ represent the rotations of the reference surface about the $\theta$- and $x$-axis. T is the time variable. The strain–displacement relationships can be written as follows [3, 8, 9]:

$$\varepsilon_x^0 = \frac{\partial u_0}{\partial x}, \quad \varepsilon_\theta^0 = \frac{\partial v_0}{R\partial\theta} + \frac{u_0}{R}\sin\varphi + \frac{w_0}{R}\cos\varphi, \gamma_{x\theta}^0 = \frac{\partial v_0}{\partial x} + \frac{\partial u_0}{R\partial\theta} - \frac{v_0}{R}\sin\varphi,$$
$$\chi_x = \frac{\partial \phi_x}{\partial x}, \quad \chi_\theta = \frac{\partial \phi_\theta}{R\partial\theta} + \frac{\phi_x}{R}\sin\varphi, \quad \chi_{x\theta} = \frac{\partial \phi_x}{R\partial\theta} + \frac{\partial \phi_\theta}{\partial x} - \frac{\phi_\theta}{R}\sin\varphi, \quad (3)$$
$$\gamma_{xz}^0 = \frac{\partial w_0}{\partial x} + \phi_x, \quad \gamma_{\theta z}^0 = \frac{\partial w_0}{R\partial\theta} - \frac{v_0}{R}\cos\varphi + \phi_\theta,$$

where $\varepsilon_x^0$, $\varepsilon_\theta^0$ and $\gamma_{x\theta}^0, \gamma_{xz}^0, \gamma_{\theta z}^0$ denote the in-plane strains at a point lying on the middle surface. $\chi_x, \chi_\theta$ and $\chi_{x\theta}$ are the curvature changes. The force and moment resultant relations to the strains in the middle surface and curvature changes are defined as in the following matrix form [3, 7–9]:

$$\begin{bmatrix} N_x \\ N_\theta \\ N_{x\theta} \\ M_x \\ M_\theta \\ M_{x\theta} \end{bmatrix} = \begin{bmatrix} A_{11} & A_{12} & A_{16} & B_{11} & B_{12} & B_{16} \\ A_{12} & A_{22} & A_{26} & B_{12} & B_{22} & B_{26} \\ A_{16} & A_{26} & A_{66} & B_{16} & B_{26} & B_{66} \\ B_{11} & B_{12} & B_{16} & C_{11} & C_{12} & C_{16} \\ B_{12} & B_{22} & B_{26} & C_{12} & C_{22} & C_{26} \\ B_{16} & B_{26} & B_{66} & C_{16} & C_{26} & C_{66} \end{bmatrix} \begin{bmatrix} \varepsilon_x^0 \\ \varepsilon_\theta^0 \\ \gamma_{x\theta}^0 \\ \chi_x \\ \chi_\theta \\ \chi_{x\theta} \end{bmatrix} \begin{bmatrix} Q_x \\ Q_\theta \end{bmatrix} = \kappa \begin{bmatrix} A_{55} & A_{45} \\ A_{45} & A_{44} \end{bmatrix} \begin{bmatrix} \gamma_{xz} \\ \gamma_{\theta z} \end{bmatrix}, \quad (4)$$

where Nx, N$\theta$, and Nx$\theta$ denote the in-plane force resultants, and Mx, M$\theta$, and Mx$\theta$ represent the bending and twisting moment resultants. Qx and Q$\theta$ are the transverse shear force resultants. $\kappa$ is the shear correction factor, and in this paper, it is set as $\kappa = 5/6$. The stiffness coefficients Aij, Bij, and Cij are defined as follows:

$$\begin{aligned} A_{ij} &= \sum_{k=1}^{N_k} \overline{Q}_{ij}^{k} \left(Z_{k+1} - Z_k\right), \ (i, j = 1, 2, 6), \\ A_{ij} &= \kappa \sum_{k=1}^{N_k} \overline{Q}_{ij}^{k} \left(Z_{k+1} - Z_k\right), \ (i, j = 4, 5), \\ B_{ij} &= \frac{1}{2} \sum_{k=1}^{N_k} \overline{Q}_{ij}^{k} \left(Z_{k+1}^2 - Z_k^2\right), \ (i, j = 1, 2, 4, 5, 6), \\ C_{ij} &= \frac{1}{3} \sum_{k=1}^{N_k} \overline{Q}_{ij}^{k} \left(Z_{k+1}^3 - Z_k^3\right), \ (i, j = 1, 2, 4, 5, 6), \end{aligned} \tag{5}$$

where $N_k$ is the number of layers. $Z_{k+1}$ and $Z_k$ denote distances from the shell reference surface to the outer and inner surfaces of the k$^{th}$ layer. The coordinate $Z_k$ of the bottom surface of the k$^{th}$ layer is expressed as a function of $x$.

$$z_k(x) = \left(-\frac{1}{2} + \frac{k-1}{N_k}\right) h(x). \tag{6}$$

The lamina stiffness coefficients $\overline{Q}_{ij}^{k}$, $(i, j = 1, 2, 4, 5, 6)$ of the k$^{th}$ layer can be obtained from the transformed stiffness matrix $\overline{\mathbf{Q}}^{k}$ ($\overline{\mathbf{Q}}^{k} = \mathbf{T}\mathbf{Q}^{k}\mathbf{T}^{T}$), in which the superscript $T$ represents the transposition operator, and $T$ is the transformation matrix, which is defined as follows:

$$\mathbf{T} = \begin{bmatrix} \cos^2\phi_f & \sin^2\phi_f & 0 & 0 & -2\sin\phi_f\cos\phi_f \\ \sin^2\phi_f & \cos^2\phi_f & 0 & 0 & 2\sin\phi_f\cos\phi_f \\ 0 & 0 & \cos\phi_f & \sin\phi_f & 0 \\ 0 & 0 & -\sin\phi_f & \cos\phi_f & 0 \\ \sin\phi_f\cos\phi_f & -\sin\phi_f\cos\phi_f & 0 & 0 & \cos^2\phi_f - \sin^2\phi_f \end{bmatrix}. \tag{7}$$

In Eq. (7), $\phi$f is the fiber orientation angle of each individual layer. $Q^k$ is the reduced stiffness matrix for each layer and is defined as follows:

$$\mathbf{Q}^{k} = \begin{bmatrix} Q_{11}^{k} & Q_{12}^{k} & 0 & 0 & 0 \\ Q_{21}^{k} & Q_{22}^{k} & 0 & 0 & 0 \\ 0 & 0 & Q_{44}^{k} & 0 & 0 \\ 0 & 0 & 0 & Q_{55}^{k} & 0 \\ 0 & 0 & 0 & 0 & Q_{66}^{k} \end{bmatrix}. \tag{8}$$

For the orthotropic materials, the components $Q_{ij}(i,j = 1,2,4,5,6)$ of the reduced stiffness matrix are defined as follows:

$$\begin{aligned} &Q_{11}^{k} = \frac{E_{11}}{1 - \mu_{12}\mu_{21}}, Q_{12}^{k} = \frac{\mu_{12}E_{22}}{1 - \mu_{12}\mu_{21}} = Q_{21}^{k}, Q_{22}^{k} = \frac{E_{22}}{1 - \mu_{12}\mu_{21}}, \\ &Q_{44}^{k} = G_{23}, Q_{55}^{k} = G_{13}, Q_{66}^{k} = G_{12}, \end{aligned} \tag{9}$$

where E11 and E22 are Yong's modulus in the principal directions of the k$^{th}$ layer, and G12, G13, and G23 are shear modulus. $\mu$12 and $\mu$21 are Poisson's ratios.

On the other hand, as the thickness of the shell are changed in the $x$-axis direction, the stiffness coefficients $A_{ij}$, $B_{ij}$, and $D_{ij}$ are the functions of $x$, and therefore, the partial derivatives of the stiffness coefficients appeared, which can be written as follows:

$$\begin{cases} \dfrac{\partial A_{ij}}{\partial x} = \sum_{k=1}^{N_k} Q_{ij}^k \left( \dfrac{\partial z_{k+1}}{\partial x} - \dfrac{\partial z_k}{\partial x} \right), & i, j = 1, 2, 6, \\ \dfrac{\partial A_{ij}}{\partial x} = k_c \sum_{k=1}^{N_k} Q_{ij}^k \left( \dfrac{\partial z_{k+1}}{\partial x} - \dfrac{\partial z_k}{\partial x} \right), & i, j = 4, 5, \\ \dfrac{\partial B_{ij}}{\partial x} = \sum_{k=1}^{N_k} Q_{ij}^k \left( z_{k+1} \dfrac{\partial z_{k+1}}{\partial x} - z_k \dfrac{\partial z_k}{\partial x} \right), & i, j = 1, 2, 6, \\ \dfrac{\partial D_{ij}}{\partial x} = \sum_{k=1}^{N_k} Q_{ij}^k \left( z_{k+1}^2 \dfrac{\partial z_{k+1}}{\partial x} - z_k^2 \dfrac{\partial z_k}{\partial x} \right), & i, j = 1, 2, 6. \end{cases} \tag{10}$$

From equation (6),

$$\frac{\partial z_k}{\partial x} = \left( -0.5 + \frac{k-1}{N_k} \right) \frac{\partial h}{\partial x}, \tag{11}$$

where $(\partial h/\partial x)$ can be obtained from equation (1).

$$\frac{\partial h}{\partial x} = -\frac{h_1 \alpha \lambda}{L} \left( \frac{x}{L} \right)^{\lambda - 1}. \tag{12}$$

*2.3. Governing Equations.* In the paper, Hamilton's principle is adopted for driving the equilibrium equations of the motion of the laminated composite conical shell, cylindrical shell, and annular plate with variable thickness [9].

$$\begin{aligned} &\frac{\partial N_x}{\partial x} + \frac{1}{R} \frac{\partial N_{x\theta}}{\partial \theta} + (N_x - N_\theta) \frac{\sin \varphi}{R} = I_0 \frac{\partial^2 u_0}{\partial t^2} + I_1 \frac{\partial^2 \phi_x}{\partial t^2}, \\ &\frac{\partial N_{x\theta}}{\partial x} + \frac{1}{R} \frac{\partial N_\theta}{\partial \theta} + Q_\theta \frac{\cos \varphi}{R} + 2N_{x\theta} \frac{\sin \varphi}{R} = I_0 \frac{\partial^2 v_0}{\partial t^2} + I_1 \frac{\partial^2 \phi_\theta}{\partial t^2}, \\ &\frac{\partial Q_x}{\partial x} + \frac{1}{R} \frac{\partial Q_\theta}{\partial \theta} + Q_x \frac{\sin \varphi}{R} - N_\theta \frac{\cos \varphi}{R} = I_0 \frac{\partial^2 w_0}{\partial t^2}, \\ &\frac{\partial M_x}{\partial x} + \frac{1}{R} \frac{\partial M_{x\theta}}{\partial \theta} + (M_x - M_\theta) \frac{\sin \varphi}{R} - Q_x = I_1 \frac{\partial^2 u_0}{\partial t^2} + I_2 \frac{\partial^2 \phi_x}{\partial t^2}, \\ &\frac{\partial M_{x\theta}}{\partial x} + \frac{1}{R} \frac{\partial M_\theta}{\partial \theta} + 2M_{x\theta} \frac{\sin \varphi}{R} - Q_\theta = I_1 \frac{\partial^2 v_0}{\partial t^2} + I_2 \frac{\partial^2 \phi_\theta}{\partial t^2}, \end{aligned} \tag{13}$$

where $I_0$, $I_1$, and $I_2$ are the mass inertia items, which can be expressed as follows:

$$[I_0, I_1, I_2] = \left( \sum_{k=1}^{N_k} \int_{Z_k}^{Z_{k+1}} \rho^k \left[ 1, z^1, z^2 \right] dz \right), \tag{14}$$

where $\rho^k$ is the density of the $k^{th}$ layer, and the cone radius at any point along its length is given by the following:

$$R(x) = R_1 + x \sin \varphi. \tag{15}$$

By substituting equations (3)–(5) into equation (13), the governing equations in terms of displacements and rotational functions of the shell can be written as follows:

$$\begin{bmatrix} L_{11} & L_{12} & L_{13} & L_{14} & L_{15} \\ L_{21} & L_{22} & L_{23} & L_{24} & L_{25} \\ L_{31} & L_{32} & L_{33} & L_{34} & L_{35} \\ L_{41} & L_{42} & L_{43} & L_{44} & L_{45} \\ L_{51} & L_{52} & L_{53} & L_{54} & L_{55} \end{bmatrix} \begin{bmatrix} u_0 \\ v_0 \\ w_0 \\ \phi_x \\ \phi_\theta \end{bmatrix} = \begin{bmatrix} 0 \\ 0 \\ 0 \\ 0 \\ 0 \end{bmatrix}, \tag{16}$$

where Lij(i, $j = 1$–5) are the differential operators. The detailed expressions can be found in appendix A. It is obvious that each of the displacement and rotation components at most has second-order derivatives.

For the certain circumferential wave number $n$, the displacements of the Eq. (16) are expressed as follows:

$$\begin{aligned} u_0(x, \theta, t) &= U(x) \cos(n\theta) e^{i\omega t}, \\ v_0(x, \theta, t) &= V(x) \sin(n\theta) e^{i\omega t}, \\ w_0(x, \theta, t) &= W(x) \cos(n\theta) e^{i\omega t}, \\ \phi_x(x, \theta, t) &= \Phi(x) \cos(n\theta) e^{i\omega t}, \\ \phi_\theta(x, \theta, t) &= \Theta(x) \sin(n\theta) e^{i\omega t}, \end{aligned} \tag{17}$$

where $U(x)$, $V(x)$, $W(x)$, $\Phi(x)$, and $\Theta(x)$ are unknown variable functions to be determined, and $\omega$ is the angular frequency. Substitute equation (17) in (16) and multiply the governing equations with R2. Then, multiply cos(n$\theta$) or sin(n$\theta$) in the governing equations, and integrate $s$ from 0 to $2\pi$.

$$\int_0^{2\pi} \cos(n\theta)\sin(n\theta)\mathrm{d}\theta = 0, \int_0^{2\pi} \cos(n\theta)\cos(n\theta)\mathrm{d}\theta = \pi, \int_0^{2\pi} \sin(n\theta)\sin(n\theta)\mathrm{d}\theta = \pi. \tag{18}$$

We can omit variable $\theta$. In this way, a two-dimension problem is transformed into a set of uncoupled one-dimension problems. Then, equation (16) can be written as follows:

$$\begin{aligned} &L_{11}^0 U + L_{11}^1 \frac{\mathrm{d}U}{\mathrm{d}x} + L_{11}^2 \frac{\mathrm{d}^2 U}{\mathrm{d}x^2} + L_{12}^0 V + L_{12}^1 \frac{\mathrm{d}V}{\mathrm{d}x} + L_{13}^0 W + L_{13}^1 \frac{\mathrm{d}W}{\mathrm{d}x} + L_{14}^0 \Phi + L_{14}^1 \frac{\mathrm{d}\Phi}{\mathrm{d}x} + L_{14}^2 \frac{\partial^2 \Phi}{\mathrm{d}x^2} + L_{15}^0 \Theta \\ &\quad + L_{15}^1 \frac{\mathrm{d}\Theta}{\mathrm{d}x} + I_0 \omega^2 R^2 U + I_1 \omega^2 R^2 \Phi = 0, \end{aligned} \tag{19a}$$

$$L_{21}^0 U + L_{21}^1 \frac{\mathrm{d}U}{\mathrm{d}x} + L_{22}^0 V + L_{22}^1 \frac{\mathrm{d}V}{\mathrm{d}x} + L_{22}^2 \frac{\mathrm{d}^2 V}{\mathrm{d}x^2} + L_{23}^0 W + L_{24}^0 \Phi + L_{24}^1 \frac{\mathrm{d}\Phi}{\mathrm{d}x} + L_{25}^0 \Theta + L_{25}^1 \frac{\mathrm{d}\Theta}{\mathrm{d}x} + L_{25}^2 \frac{\mathrm{d}^2 \Theta}{\mathrm{d}x^2} + I_0 R^2 \omega^2 V + I_1 \omega^2 R^2 \Theta = 0, \tag{19b}$$

$$L_{31}^0 U + L_{31}^1 \frac{\mathrm{d}U}{\mathrm{d}x} + L_{32}^0 V + L_{33}^0 W + L_{33}^1 \frac{\mathrm{d}W}{\mathrm{d}x} + L_{33}^2 \frac{\mathrm{d}^2 W}{\mathrm{d}x^2} + L_{34}^0 \Phi + L_{34}^1 \frac{\mathrm{d}\Phi}{\mathrm{d}x} + L_{35}^0 \Theta - I_0 R^2 \omega^2 W = 0, \tag{19c}$$

$$\begin{aligned} &L_{41}^0 U + L_{41}^1 \frac{\mathrm{d}U}{\mathrm{d}x} + L_{41}^2 \frac{\mathrm{d}^2 U}{\mathrm{d}x^2} + L_{42}^0 V + L_{42}^1 \frac{\mathrm{d}V}{\mathrm{d}x} + L_{43}^0 W + L_{43}^1 \frac{\mathrm{d}W}{\mathrm{d}x} + L_{44}^0 \Phi + L_{44}^1 \frac{\mathrm{d}\Phi}{\mathrm{d}x} + L_{44}^2 \frac{\mathrm{d}^2 \Phi}{\mathrm{d}x^2} + L_{45}^0 \Theta + L_{45}^1 \frac{\mathrm{d}\Theta}{\mathrm{d}x} \\ &\quad + I_1 R^2 \omega^2 U + I_2 R^2 \Phi = 0, \end{aligned} \tag{19d}$$

$$L_{51}^0 U + L_{51}^1 \frac{\mathrm{d}U}{\mathrm{d}x} + L_{52}^0 V + L_{52}^1 \frac{\mathrm{d}^2 V}{\mathrm{d}x^2} + L_{53}^0 W + L_{54}^0 \Phi + L_{54}^1 \frac{\mathrm{d}\Phi}{\mathrm{d}x} + L_{55}^0 \Theta + L_{55}^1 \frac{\mathrm{d}\Theta}{\mathrm{d}x} + L_{55}^2 \frac{\mathrm{d}^2 \Theta}{\mathrm{d}x^2} + I_1 \omega^2 R^2 V + I_2 \omega^2 R^2 \Theta = 0. \tag{19e}$$

The detailed expressions of the coefficient items Lijk can be found in Appendix B.

Disposing the boundary condition in vibration problems has always been one of the most challenging and important issues. In this paper, for generalizing the boundary conditions, the artificial springs technique has been employed. Therefore, the boundary conditions are modeled using three kinds of linear springs (ku, kv, kw) and two kinds of rotational springs (k$\varphi$, k$\theta$) by assigning that these springs are at proper stiffness. The boundary condition equations for the laminated composite conical shell, cylindrical shell, and annular plate with variable thickness can be expressed as follows:

$$\begin{aligned} x = 0: &\begin{cases} N_x - k_u^{x0} u = 0, \\ N_{x\theta} - k_v^{x0} v = 0, \\ Q_x - k_w^{x0} w = 0, \\ M_x - k_\varphi^{x0} \phi_x = 0, \\ M_{x\theta} - k_\theta^{x0} \phi_\theta = 0, \end{cases} \\ x = L: &\begin{cases} N_x + k_u^{x1} u = 0, \\ N_{x\theta} + k_v^{x1} v = 0, \\ Q_x + k_w^{x1} w = 0, \\ M_x + k_\varphi^{x1} \phi_x = 0, \\ M_{x\theta} + k_\theta^{x1} \phi_\theta = 0. \end{cases} \end{aligned} \tag{20}$$

By substituting equations (3), (4), and (17) into (20), the generalized boundary condition equations can be obtained. For example, by applying $x = 0$, the boundary condition equations at the left boundary can be written as follows:

$$\begin{aligned}
&A_{12}\sin\varphi U - k_u^{x0}RU + A_{11}R\frac{dU}{dx} + A_{12}nV + A_{12}\cos\varphi W + B_{12}\sin\varphi\Phi + B_{11}R\frac{d\Phi}{dx} + B_{12}n\Theta \\
&= 0 - A_{66}nU - A_{66}\sin\varphi V - k_v^{x0}RV + A_{66}R\frac{dV}{dx} - B_{66}n\Phi - B_{66}\sin\varphi\Theta + B_{66}R\frac{d\Theta}{dx} = 0 - k_w^{x0}RW + \kappa A_{55}R\frac{dW}{dx} + \kappa A_{55}R\Phi \\
&= 0B_{12}\sin\varphi U + B_{11}R\frac{dU}{dx} + B_{12}nV + B_{12}\cos\varphi W + D_{12}\sin\varphi\Phi - k_\varphi^{x0}R\Phi + D_{11}R\frac{d\Phi}{dx} + D_{12}n\Theta = 0 - B_{66}nU \\
&\quad - B_{66}\sin\varphi V + B_{66}R\frac{dV}{dx} - D_{66}n\Phi - D_{66}\sin\varphi\Theta - k_\theta^{x0}R\Theta + D_{66}R\frac{d\Theta}{dx} = 0.
\end{aligned} \tag{21}$$

Similarly, the boundary condition equations of the right boundary can be obtained by applying $x = L$ in Eq. (21). Therefore, the generalized boundary equations of shell according to the spring stiffness can be obtained, and the various boundary conditions can be modeled by setting the appropriate values of the spring stiffness.

*2.4. Implementation of the HWDM.* In the current study, Haar wavelet series are employed for the discretization of the derivatives in governing the equations of the whole system, including boundary conditions. The basic theories of Haar wavelet have been introduced in Xie's studies [4–6, 9, 11, 71] and author's studies [67, 68, 72–75]. Therefore, in this paper, the explanation for Haar wavelet is downplayed.

In the HWDM, the highest order derivatives of the displacement components are defined by the Haar wavelet series, and the lower order derivatives can be obtained by integrating Haar wavelet series. The highest order derivative of the displacements in the governing equations of shell is the second order, which can be expressed by means of the Haar wavelet series as follows:

$$\begin{aligned}
&\frac{d^2U(\xi)}{d\xi^2} = \sum_{i=1}^{2M} a_i h_i(\xi), \frac{d^2V(\xi)}{d\xi^2} = \sum_{i=1}^{2M} b_i h_i(\xi), \frac{d^2W(\xi)}{d\xi^2} = \sum_{i=1}^{2M} c_i h_i(\xi), \\
&\frac{d^2\Phi(\xi)}{d\xi^2} = \sum_{i=1}^{2M} d_i h_i(\xi), \frac{d^2\Theta(\xi)}{d\xi^2} = \sum_{i=1}^{2M} e_i h_i(\xi),
\end{aligned} \tag{22}$$

where $a_i$, $b_i$, $c_i$, and $d_i$ are the unknown coefficients of the Haar wavelets. The first-order derivatives of displacements are obtained by integrating equations (22) and the displacement functions can be obtained by integrating the above result again. The first-order derivatives of displacements and displacement functions are expressed as follows:

$$\frac{dU(\xi)}{d\xi} = \sum_{i=1}^{2M} a_i P_{1,i}(\xi) + \frac{dU(0)}{d\xi}, U(\xi) = \sum_{i=1}^{2M} a_i P_{2,i}(\xi) + \xi\frac{dU(0)}{d\xi} + U(0),$$

$$\frac{dV(\xi)}{d\xi} = \sum_{i=1}^{2M} a_i P_{1,i}(\xi) + \frac{dV(0)}{d\xi}, V(\xi) = \sum_{i=1}^{2M} b_i P_{2,i}(\xi) + \xi\frac{dV(0)}{d\xi} + V(0),$$

$$\frac{dW(\xi)}{d\xi} = \sum_{i=1}^{2M} c_i P_{1,i}(\xi) + \frac{dW(0)}{d\xi}, W(\xi) = \sum_{i=1}^{2M} c_i P_{2,i}(\xi) + \xi\frac{dW(0)}{d\xi} + W(0), \tag{23}$$

$$\frac{d\Phi(\xi)}{d\xi} = \sum_{i=1}^{2M} d_i P_{1,i}(\xi) + \frac{d\Phi(0)}{d\xi}, \Phi(\xi) = \sum_{i=1}^{2M} d_i P_{2,i}(\xi) + \xi\frac{d\Phi(0)}{d\xi} + \Phi(0),$$

$$\frac{d\Theta(\xi)}{d\xi} = \sum_{i=1}^{2M} e_i P_{1,i}(\xi) + \frac{d\Theta(0)}{d\xi}, \Theta(\xi) = \sum_{i=1}^{2M} e_i P_{2,i}(\xi) + \xi\frac{d\Theta(0)}{d\xi} + \Theta(0).$$

In equations (22) and (23), hi(ξ) is the Haar wavelet series and P1,i(ξ) and P2,i(ξ) are their integrals.

Equations (22) and (23) can be expressed in the discretized matrix form as follows:

$$\frac{\mathrm{d}^2\mathbf{U}}{\mathrm{d}\xi^2} = \mathbf{H}_1\mathbf{a} + \mathbf{H}_{11}\mathbf{f}, \quad \frac{d\mathbf{U}}{d\xi} = \mathbf{P}_1\mathbf{a} + \mathbf{P}_{11}\mathbf{f}, \quad \mathbf{U} = \mathbf{P}_2\mathbf{a} + \mathbf{P}_{22}\mathbf{f},$$

$$\frac{\mathrm{d}^2\mathbf{V}}{\mathrm{d}\xi^2} = \mathbf{H}_1\mathbf{b} + \mathbf{H}_{11}\mathbf{g}, \quad \frac{\mathrm{d}\mathbf{V}}{\mathrm{d}\xi} = \mathbf{P}_1\mathbf{b} + \mathbf{P}_{11}\mathbf{g}, \quad \mathbf{V} = \mathbf{P}_2\mathbf{b} + \mathbf{P}_{22}\mathbf{g},$$

$$\frac{\mathrm{d}\mathbf{W}}{\mathrm{d}\xi} = \mathbf{P}_1\mathbf{c} + \mathbf{P}_{11}\mathbf{h}, \quad \mathbf{W} = \mathbf{P}_2\mathbf{c} + \mathbf{P}_{22}\mathbf{h}, \tag{24}$$

$$\frac{\mathrm{d}^2\mathbf{\Phi}}{d\xi^2} = \mathbf{H}_1\mathbf{d} + \mathbf{H}_{11}\mathbf{k}, \quad \frac{\mathrm{d}\mathbf{\Phi}}{\mathrm{d}\xi} = \mathbf{P}_1\mathbf{d} + \mathbf{P}_{11}\mathbf{k}, \quad \mathbf{\Phi} = \mathbf{P}_2\mathbf{d} + \mathbf{P}_{22}\mathbf{k},$$

$$\frac{\mathrm{d}^2\Theta}{\mathrm{d}\xi^2} = \mathbf{H}_1\mathbf{e} + \mathbf{H}_{11}\mathbf{l}, \quad \frac{\mathrm{d}\Theta}{\mathrm{d}\xi} = \mathbf{P}_1\mathbf{e} + \mathbf{P}_{11}\mathbf{l}, \quad \Theta = \mathbf{P}_2\mathbf{e} + \mathbf{P}_{22}\mathbf{l},$$

where Haar wavelet H and its integrals P1, P2 are defined in the matrix form as follows:

$$\mathbf{H}_1 = \begin{bmatrix} h_1(\xi_1) & h_2(\xi_1) & \cdots & h_n(\xi_1) \\ h_1(\xi_2) & h_2(\xi_2) & \cdots & h_n(\xi_2) \\ \vdots & \vdots & \ddots & \vdots \\ h_1(\xi_n) & h_2(\xi_n) & \cdots & h_n(\xi_n) \end{bmatrix}, \mathbf{H}_{11} = \begin{bmatrix} 0 & 0 \\ 0 & 0 \\ \vdots & \vdots \\ 0 & 0 \end{bmatrix}, \tag{25}$$

$$\mathbf{P}_1 = \begin{bmatrix} P_{1,1}(\xi_1) & P_{1,2}(\xi_1) & \cdots & P_{1,n}(\xi_1) \\ P_{1,1}(\xi_2) & P_{1,2}(\xi_2) & \cdots & P_{1,n}(\xi_2) \\ \vdots & \vdots & \ddots & \vdots \\ P_{1,1}(\xi_n) & P_{1,2}(\xi_n) & \cdots & P_{1,n}(\xi_n) \end{bmatrix}, \mathbf{P}_{11} = \begin{bmatrix} 1 & 0 \\ 1 & 0 \\ \vdots & \vdots \\ 1 & 0 \end{bmatrix}, \tag{26}$$

$$\mathbf{P}_2 = \begin{bmatrix} P_{2,1}(\xi_1) & P_{2,2}(\xi_1) & \cdots & P_{2,n}(\xi_1) \\ P_{2,1}(\xi_2) & P_{2,2}(\xi_2) & \cdots & P_{2,n}(\xi_2) \\ \vdots & \vdots & \ddots & \vdots \\ P_{2,1}(\xi_n) & P_{2,2}(\xi_n) & \cdots & P_{2,n}(\xi_n) \end{bmatrix}, \mathbf{P}_{22} = \begin{bmatrix} \xi_1 & 1 \\ \xi_2 & 1 \\ \vdots & \vdots \\ \xi_n & 1 \end{bmatrix}, \tag{27}$$

and notations are defined as follows:

$$\begin{aligned} &\mathbf{U} = [U(\xi_1), U(\xi_2), \cdots, U(\xi_n)]^T, \mathbf{a} = [a_1, a_2, \cdots, a_n]^T, \mathbf{f} = \left[\frac{dU(\xi_0)}{d\xi}, U(\xi_0)\right]^T \mathbf{V} = [V(\xi_1), V(\xi_2), \cdots, V(\xi_n)]^T, \\ &\mathbf{b} = [b_1, b_2, \cdots, b_n]^T, \mathbf{g} = \left[\frac{dV(\xi_0)}{d\xi}, V(\xi_0)\right]^T \mathbf{W} = [W(\xi_1), W(\xi_2), \cdots, W(\xi_n)]^T, \mathbf{c} = [c_1, c_2, \cdots, c_n]^T, \\ &\mathbf{h} = \left[\frac{dW(\xi_0)}{d\xi}, W(\xi_0)\right]^T \mathbf{\Phi} = [\Phi(\xi_1), \Phi(\xi_2), \cdots, \Phi(\xi_n)]^T, \mathbf{d} = [d_1, d_2, \cdots, d_n]^T, \mathbf{k} = \left[\frac{d\Phi(\xi_0)}{d\xi}, \Phi(\xi_0)\right]^T \\ &\Theta = [\Theta(\xi_1), \Theta(\xi_2), \cdots, \Theta(\xi_n)]^T, \mathbf{e} = [e_1, e_2, \cdots, e_n]^T, \mathbf{l} = \left[\frac{d\Theta(\xi_0)}{d\xi}, \Theta(\xi_0)\right]^T, \end{aligned} \tag{28}$$

where, *f*, *g*, *h*, *k*, and *l* indicate the integral constants, which can be obtained by applying the boundary condition. The highest order of the displacements of boundary condition equations is the first-order, and the first-order derivatives and displacements in Eq (23) are calculated when $\xi = 0$ and $\xi = 1$. The discretization of the boundary condition equation can be manipulated in the same way as that of the displacement, and it can be written in the matrix form as follows:

$$\begin{aligned} &\frac{\mathrm{d}\mathbf{U_b}}{\mathrm{d}\xi} = \mathbf{P_{b1}a} + \mathbf{P_{b11}f}, \frac{\mathrm{d}\mathbf{V_b}}{\mathrm{d}\xi} = \mathbf{P_{b1}b} + \mathbf{P_{b11}g}, \frac{\mathrm{d}\mathbf{W_b}}{\mathrm{d}\xi} = \mathbf{P_{b1}c} + \mathbf{P_{b11}h}, \\ &\frac{\mathrm{d}\mathbf{\Phi_b}}{\mathrm{d}\xi} = \mathbf{P_{b1}d} + \mathbf{P_{b11}k}, \frac{\mathrm{d}\mathbf{\Theta_b}}{\mathrm{d}\xi} = \mathbf{P_{b1}e} + \mathbf{P_{b11}l}, \end{aligned} \tag{29}$$

$$\begin{aligned} &\mathbf{U_b} = \mathbf{P_{b2}a} + \mathbf{P_{b22}f}, \mathbf{V_b} = \mathbf{P_{b2}b} + \mathbf{P_{b22}g}, \mathbf{W_b} = \mathbf{P_{b2}c} + \mathbf{P_{b22}h}, \\ &\mathbf{\Phi_b} = \mathbf{P_{b2}d} + \mathbf{P_{b22}k}, \mathbf{\Theta_b} = \mathbf{P_{b2}e} + \mathbf{P_{b22}l}, \end{aligned} \tag{30}$$

where notations are defined as follows:

$$\mathbf{P_{b1}} = \begin{bmatrix} p_{1,1}(0) & p_{1,2}(0) & \cdots & p_{1,n}(0) \\ p_{1,1}(1) & p_{1,2}(1) & \cdots & p_{1,n}(1) \end{bmatrix}, \mathbf{P_{b1}} = \begin{bmatrix} 1 & 1 \\ 1 & 1 \end{bmatrix}, \tag{31}$$

$$\mathbf{P_{b2}} = \begin{bmatrix} p_{2,1}(0) & p_{2,2}(0) & \cdots & p_{2,n}(0) \\ p_{2,1}(1) & p_{2,2}(1) & \cdots & p_{2,n}(1) \end{bmatrix}, \mathbf{P_{b2}} = \begin{bmatrix} \xi_0 & 1 \\ \xi_1 & 1 \end{bmatrix}, \tag{32}$$

Therefore, the equations of motion of the total systems of the laminated composite structures, including the boundary condition, are discretized using HWDM and can be expressed in the matrix form as follows:

$$\begin{bmatrix} \mathbf{K}_{d\,d} & \mathbf{K}_{db} \\ \mathbf{K}_{b\,d} & \mathbf{K}_{bb} \end{bmatrix} \begin{bmatrix} \mathbf{A}_d \\ \mathbf{A}_b \end{bmatrix} - \omega^2 \begin{bmatrix} \mathbf{M}_{d\,d} & \mathbf{M}_{db} \\ 0 & 0 \end{bmatrix} \begin{bmatrix} \mathbf{A}_d \\ \mathbf{A}_b \end{bmatrix} = 0, \tag{33}$$

$$\mathbf{A}_d = [\mathbf{a}, \mathbf{b}, \mathbf{c}, \mathbf{d}, \mathbf{e}]^T, \mathbf{A}_b = [\mathbf{f}, \mathbf{g}, \mathbf{h}, \mathbf{k}, \mathbf{l}]^T, \tag{34}$$

where subscripts *d* and *b* indicate the discrete equilibrium equations of motion and the boundary conditions. Ab at both sides of equation (33) can be eliminated by performing some algebraic manipulations, and the standard characteristic equation is expressed as follows:

$$\left[\mathbf{K}_{dd} - \mathbf{K}_{db}\mathbf{K}_{bb}^{-1}\mathbf{K}_{bd}\right]\mathbf{A}_d = \omega^2\left[\mathbf{M}_{dd} - \mathbf{M}_{db}\mathbf{K}_{bb}^{-1}\mathbf{K}_{bd}\right]\mathbf{A}_d. \tag{35}$$

Upon further simplification of the above equation, the matrix expressions obtained are as follows:

$$\left(\mathbf{K} - \omega^2 \mathbf{M}\right)\mathbf{A}_d = 0, \tag{36}$$

where K and $M$ are stiffness and mass matrixes of the structure, respectively.

## 3. Numerical Example and Discussion

In this section, some numerical examples are presented to analyze the free vibration of the conical shell, cylindrical shell, and annular plate. To verify the accuracy and reliability of the proposed method, different boundary conditions, thickness profiles, and geometric parameters are considered. The material properties in this research are as follows: E22 = 10 GPa, E11 = open, G12 = G13 = 6 GPa, G23 = 5 GPa, $\mu$12 = 0.25, $\rho$ = 1500 kg/m3. Then, for convenience, the frequency parameter is defined as follows: $\Omega n,m = \omega R1(\rho/E22)$ 1/2, in which the subscripts $n$ and $m$ represent the circumferential wave number and longitudinal mode number, respectively.

*3.1. Convergence.* In theory, Haar wavelet series can be infinitely expanded. However, for the accuracy of solution and efficiency of calculation, it must be truncated at an appropriate finite number. Therefore, convergence studies are needed to establish the number of terms that should be used to obtain accurate results. The convergence criterion of the present method for a four-layered, cross-ply [0°/90°/0°/90°] C–C conical shell with respect to a different maximal level of resolution $J$ is examined in Figure 4. The geometric parameters are as follows: $L = 2$m, $R1 = 1$m, $\varphi = 30°$, $h1 = 0.05$ m, and the thickness variation parameters are the same as $\alpha = 0.5$, $\lambda = 1$. Hence, according to Figure 4, it can be deduced that the present solution provides rapid convergence high accuracy even at low level of the resolution $J$, so that the computational cost in HWDM is significantly reduced.

It is also observed that when the resolution $J$ reaches a certain value, the results remain almost unchanged. Hence, the maximal level of resolution $J$ for the following numerical examples is uniformly chosen as $J = 7$. As mentioned in the theoretical formulation, the artificial spring technique is introduced for the generalization of boundary conditions in this paper, and the boundary conditions are changed according to the stiffness values of the artificial spring, such as ku, kv, kw, k$\varphi$, and k$\theta$. Therefore, the stiffness values must be selected to determine the classical and elastic boundary conditions. Figure 5 shows the change of frequency parameter of the laminated composite structure by increasing the stiffness values of the artificial spring. The geometric parameters of the structures are the same as Figure 4. To study the influence of individual spring stiffness value, in addition to the considered spring stiffness value, the other four spring stiffness values are selected as infinite (1020). In Figure 5, regardless of the structures (conical shell, cylindrical shell, and annular plate), the frequency parameters are almost unchanged in the region, where the stiffness value is less than 104 or more than 1012. Then, it is increased in the stiffness values of 104 to 1012. Therefore, the stiffness values of artificial spring for the fixed and elastic boundary conditions are shown in Table 1. For the convenience of the presentation, classical boundary conditions, such as the clamped, free, simply-supported, and shear-diaphragm are indicated with C, F, SS, and SD, respectively. Also, three kinds of elastic boundary conditions are considered in this example, which are denoted as EI, EII, and EIII.

*3.2. Validation.* In the previous subsection, through the convergence study, the maximal level of resolution and the stiffness values of the boundary elastic spring are obtained to analyze the free vibration of the laminated composite conical and cylindrical shells and the annular plate. In here, the accuracy of the proposed method is verified by the numerical comparison. Firstly, the frequency parameters of the laminated composite conical and cylindrical shells and the annular plate with even thickness by the proposed method are compared with the numericalresults ofliterature. Table 2–4 show Table 3, the frequency parameters of the laminated composite conical and cylindrical shells and the annular plate with different boundary conditions and material properties by the proposed method in comparison with the results of literature. In Table 2–4, the result by the proposed method is very consistent with that of the literature. In the comparison study, the result by the proposed method is also consistent with that of the literature.

The main purpose of this paper is to analyze the free vibration of the laminated composite structure with the varying thickness. Hence, the accuracy of the proposed method on these structures must be verified. Because of the lack of literature studying the free vibration of laminated composite structures with the varying thickness, the comparison study is onlyconducted incomparison with ABAQUS. Tables 5–7 show Table 6 the comparison result of natural frequencies of the laminated composite conical shell, cylindrical shell, and annular plate with varying thickness under different boundary conditions. The material properties are the same as Table 4. The parameters for thickness profile are $\alpha = 0.5$, $\lambda = 1$, and the fiber angle is [90°/0°]. The geometric parameters are $R = 0.5$ m, $h1 = 0.05$ m in Table 5, $R1 = 0.5$ m, $h1 = 0.05$ m, $L = 3$m in Table 6, and $R1 = 0.5$ m, $h1 = 0.05$ m in Table 7. For ABAQUS analysis, an element type S4R is used. In cylindrical shells, when L/R = 2 and L/R = 5, the number of elements is 3150 and 7850, respectively.

In Tables 5–7, regardless of the geometric dimensions and boundary conditions, the natural frequencies of the laminated composite conical shell, cylindrical shell, and annular plate with varying thickness by the proposed method are very consistent with those by FEM. From this, the proposed method is a reasonable method, which can ensure a high accuracy in the free vibration analysis of the conical shell, cylindrical shell, and annular plate with varying thickness.

*3.3. Parametric Studies.* In the last section, parametric studies are carried out to investigate the effects of material properties, geometrical parameters, and boundary conditions on the free vibration of the laminated composite

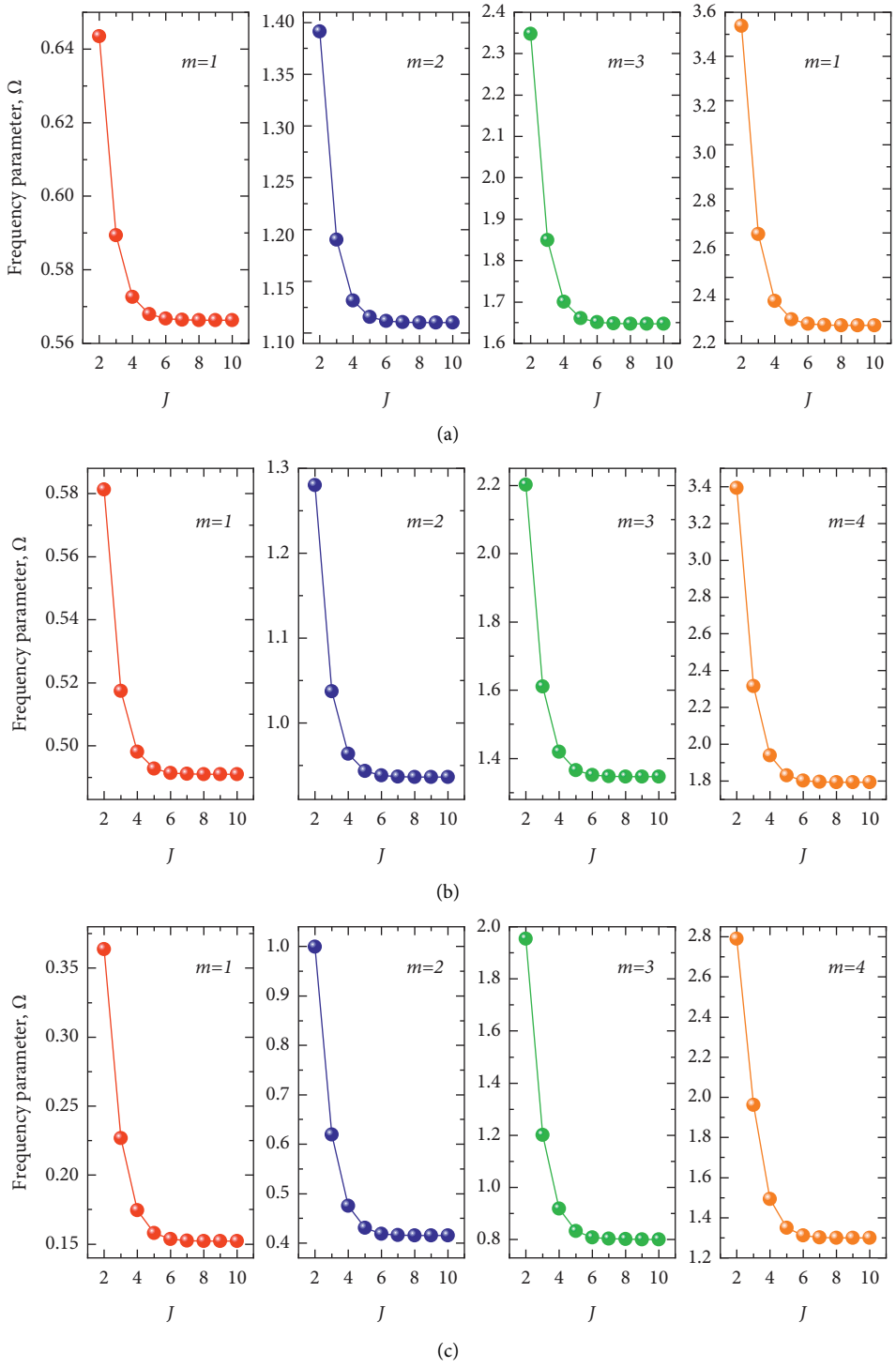


Figure 4: Convergence of frequency parameters Ω for the laminated composite structures with variable thickness and C–C boundary condition according to maximal level of resolution J ($n = 2$), (a) conical shell, (b) cylindrical shell, and (c) annular plate.

conical shell, cylindrical shelland annular plate with variablethickness. Tables 8–10 show Table 9 the frequency parameters of the conical shell, cylindrical shell, and annular plate with varying thickness according to different classic and elastic boundary conditions. The material properties are E11/$E22 = 15$, $\phi f = [0^\circ/90^\circ/0^\circ]$, and the parameters for the thickness profile are $\alpha = 0.5$, $\lambda = 1$. The geometric parameters are $R1 = 1$m, $L = 2$m, $\varphi = 45^\circ$, $h1 = 0.05$ m in the conical shell, $R = 1$m, $L = 2$m, $h1 = 0.05$ m in the cylindrical shell and $R1 = 1$m, $R2 = 3$m, $h1 = 0.05$ m in the annular plate. In Tables 8–10, the change of boundary condition affects the frequency parameters of the laminated composite structure with varying thickness explicitly. In particular, regardless of the structure, the frequency parameter is the largest in C–C

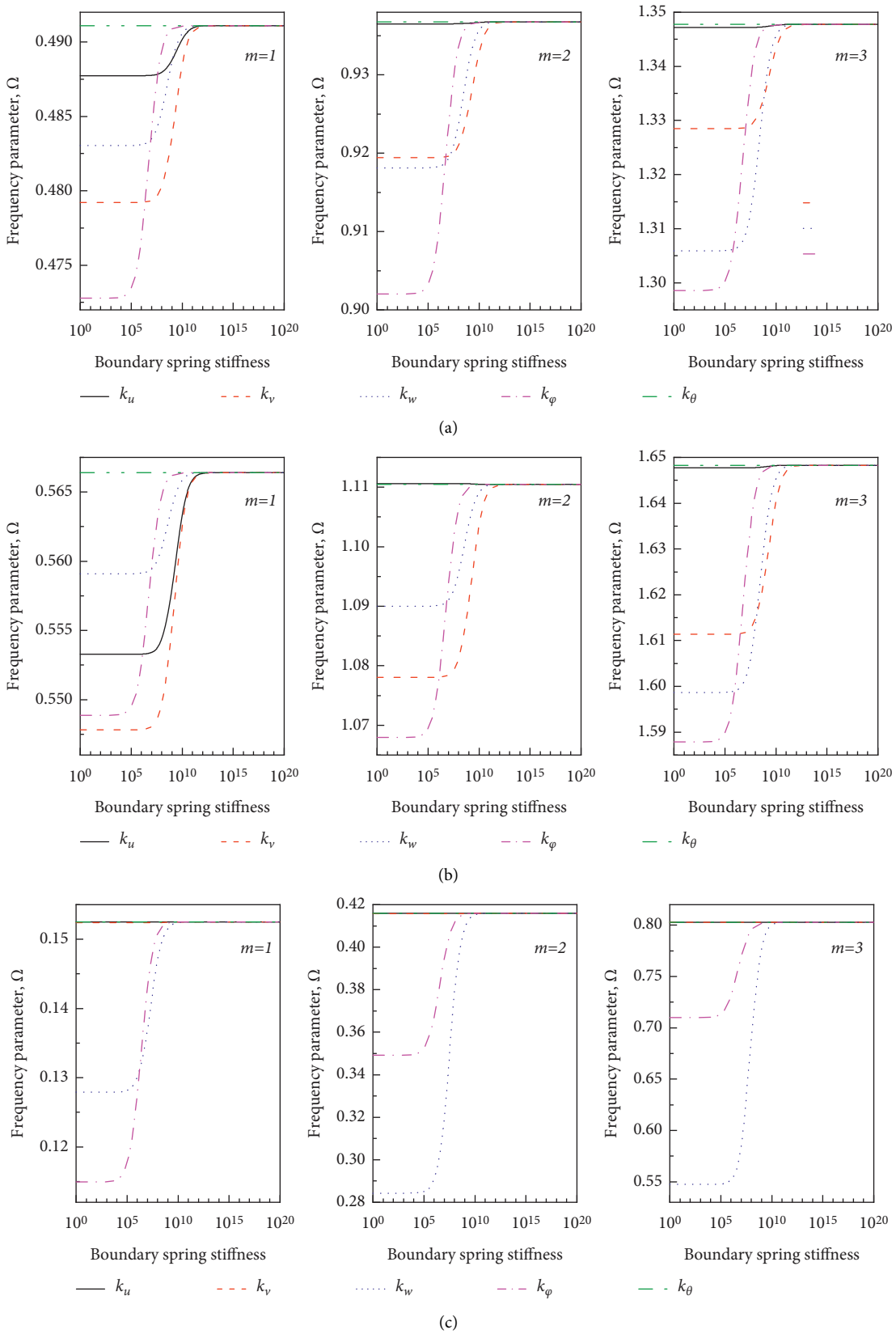


Figure 5: Variation of the frequency parameters Ω of laminated structures with variable thickness according to the boundary spring stiffness, (a) conical shell, (b) cylindrical shell, and (c) annular plate.

Table 1: The corresponding values of the spring stiffness for general boundary conditions.

| Boundary conditions | Corresponding spring stiffness values | | | | |
|---|---|---|---|---|---|
| | Ku, N/m | kv, N/m | kw, N/m | k$\varphi$, Nm/rad | k$\theta$, Nm/rad |
| F | 0 | 0 | 0 | 0 | 0 |
| C | 1014 | 1014 | 1014 | 1014 | 1014 |
| SS | 1014 | 1014 | 1014 | 0 | 1014 |
| SD | 0 | 1014 | 1014 | 0 | 1014 |
| EI | 108 | 108 | 108 | 1014 | 1014 |
| EII | 1014 | 1014 | 1014 | 108 | 108 |
| EIII | 108 | 108 | 108 | 108 | 108 |

Table 2: Comparison of the fundamental frequency parameters $\Omega = \omega L2/100h(\rho/E2)1/2$ of two certain cross-ply laminated cylindrical shells with different length–radius ratios and boundary conditions ($R = 1$m, h/R = 0.2, E22 = 1 GPa, E11 = 40 GPa, $\mu 12 = 0.25$, G12 = 6 GPa, G13 = G23 = 5 GPa, $\rho = 1600$ kg/m3).

| Lamination schemes | Refs | L/R = 1 | | | | L/R = 2 | | | |
|---|---|---|---|---|---|---|---|---|---|
| | | C–C | C–F | SS-SS | SS-C | C–C | C–F | SS-SS | SS-C |
| [0°/90°] | Ref. [1] | 0.1085 | 0.0444 | 0.0804 | 0.0938 | 0.1928 | 0.0921 | 0.1556 | 0.1726 |
| | Ref. [1] | 0.1002 | 0.0435 | 0.0791 | 0.0893 | 0.1876 | 0.0914 | 0.1552 | 0.1697 |
| | Ref. [1] | 0.1048 | 0.0480 | 0.0866 | 0.1152 | 0.2120 | 0.0938 | 0.1630 | 0.1841 |
| | Ref. [2] | 0.0982 | 0.0396 | 0.0766 | 0.0823 | 0.1737 | 0.0872 | 0.1519 | 0.1661 |
| | Ref. [3] | 0.0982 | 0.0396 | 0.0881 | 0.0921 | 0.1738 | 0.0872 | 0.1578 | 0.1639 |
| | Present | 0.0962 | 0.0394 | 0.0884 | 0.0908 | 0.1723 | 0.0871 | 0.1581 | 0.1631 |
| [0°/90°/0°] | Ref. [1] | 0.1192 | 0.0506 | 0.1007 | 0.1087 | 0.2191 | 0.0995 | 0.1777 | 0.1972 |
| | Ref. [1] | 0.1093 | 0.0495 | 0.1004 | 0.1036 | 0.2129 | 0.0988 | 0.1779 | 0.1945 |
| | Ref. [1] | 0.2049 | 0.0669 | 0.1479 | 0.1850 | 0.3338 | 0.1099 | 0.2073 | 0.2662 |
| | Ref. [2] | 0.1083 | 0.0483 | 0.0996 | 0.1025 | 0.2083 | 0.0914 | 0.1722 | 0.1950 |
| | Ref. [3] | 0.1086 | 0.0483 | 0.0996 | 0.1028 | 0.2084 | 0.0912 | 0.1726 | 0.1991 |
| | Present | 0.1042 | 0.0471 | 0.0967 | 0.0993 | 0.2018 | 0.0903 | 0.1706 | 0.1855 |

Table 3: Comparison of the frequency parameters $\Omega = \omega R2(\rho h/A11)1/2$ for the antisymmetric cross-ply [0°/90°]10 conical shell with different boundary conditions. ($R1 = 1$m, E22 = 5 GPa, E11 = 75 GPa, $\mu 12 = 0.25$, G12 = 5 GPa, G13 = G23 = 3.846 GPa, $\rho = 1600$ kg/m3, $\varphi = 30°$, $m = 1$).

| h/R2 | n | SS-C | | | SS-SS | | | SS-SD | | | SS-F | | |
|---|---|---|---|---|---|---|---|---|---|---|---|---|---|
| | | Ref. [8] | Ref. [7] | Present | Ref. [8] | Ref. [7] | Present | Ref. [8] | Ref. [7] | Present | Ref. [8] | Ref. [7] | Present |
| 0.01 | 0 | 1.00630 | 1.00876 | 1.00882 | 0.96688 | 0.9727 | 0.97275 | 0.95285 | 0.95855 | 0.95861 | 0.65316 | 0.65283 | 0.65285 |
| | 1 | 0.78588 | 0.78732 | 0.78738 | 0.76234 | 0.76504 | 0.76507 | 0.75959 | 0.76234 | 0.76237 | 0.39729 | 0.39879 | 0.39880 |
| | 2 | 0.57234 | 0.57368 | 0.57376 | 0.54541 | 0.54805 | 0.54809 | 0.5454 | 0.54803 | 0.54807 | 0.24841 | 0.24872 | 0.24873 |
| | 3 | 0.44787 | 0.44942 | 0.44952 | 0.41519 | 0.41843 | 0.41847 | 0.41393 | 0.41714 | 0.41718 | 0.17660 | 0.17710 | 0.17711 |
| | 4 | 0.3766 | 0.37842 | 0.37853 | 0.33887 | 0.34284 | 0.34289 | 0.33581 | 0.33974 | 0.33978 | 0.14164 | 0.14234 | 0.14235 |
| | 5 | 0.33859 | 0.34067 | 0.34078 | 0.29725 | 0.30190 | 0.30196 | 0.29276 | 0.29738 | 0.29742 | 0.13293 | 0.13289 | 0.13290 |
| | 6 | 0.32529 | 0.32758 | 0.3277 | 0.28221 | 0.28738 | 0.28744 | 0.27697 | 0.28211 | 0.28215 | 0.14394 | 0.14482 | 0.14483 |
| | 7 | 0.33292 | 0.33536 | 0.33547 | 0.28989 | 0.29535 | 0.29541 | 0.28461 | 0.29004 | 0.29007 | 0.17237 | 0.17325 | 0.17325 |
| | 8 | 0.35884 | 0.36137 | 0.36148 | 0.31692 | 0.32252 | 0.32257 | 0.31210 | 0.31764 | 0.31766 | 0.21241 | 0.21328 | 0.21328 |
| | 9 | 0.40040 | 0.40301 | 0.40310 | 0.35967 | 0.36537 | 0.36542 | 0.35549 | 0.36111 | 0.36113 | 0.26088 | 0.26175 | 0.26175 |
| 0.05 | 0 | 1.23197 | 1.23260 | 1.23264 | 1.10807 | 1.11131 | 1.11134 | 1.10207 | 1.10264 | 1.10272 | 0.65301 | 0.65277 | 0.65285 |
| | 1 | 1.02285 | 1.02304 | 1.02311 | 0.90038 | 0.90203 | 0.90209 | 0.90127 | 0.90148 | 0.90155 | 0.40042 | 0.40033 | 0.40038 |
| | 2 | 0.88337 | 0.88347 | 0.88354 | 0.73666 | 0.73800 | 0.73806 | 0.73689 | 0.73699 | 0.73705 | 0.25726 | 0.2572 | 0.25725 |
| | 3 | 0.83466 | 0.83479 | 0.83485 | 0.67391 | 0.67542 | 0.67547 | 0.67191 | 0.67203 | 0.67207 | 0.21918 | 0.21923 | 0.21927 |
| | 4 | 0.84227 | 0.84249 | 0.84254 | 0.68051 | 0.68242 | 0.68247 | 0.67709 | 0.67732 | 0.67736 | 0.26858 | 0.26881 | 0.26884 |
| | 5 | 0.89573 | 0.89610 | 0.89615 | 0.74256 | 0.74505 | 0.74509 | 0.73879 | 0.73919 | 0.73922 | 0.37688 | 0.37729 | 0.37731 |
| | 6 | 0.99044 | 0.99101 | 0.99105 | 0.85036 | 0.85357 | 0.85361 | 0.84701 | 0.84761 | 0.84763 | 0.51858 | 0.51918 | 0.51919 |
| | 7 | 1.12070 | 1.12149 | 1.12152 | 0.99397 | 0.99799 | 0.99802 | 0.99140 | 0.99223 | 0.99225 | 0.68156 | 0.68234 | 0.68235 |
| | 8 | 1.27955 | 1.28058 | 1.28061 | 1.16426 | 1.16910 | 1.16912 | 1.16258 | 1.16364 | 1.16365 | 0.85967 | 0.86064 | 0.86065 |
| | 9 | 1.46023 | 1.46149 | 1.46151 | 1.35384 | 1.35950 | 1.35952 | 1.35302 | 1.35430 | 1.35431 | 1.04914 | 1.05029 | 1.05030 |

Table 3: Continued.

| h/R2 | n | SS-C | | | SS-SS | | | SS-SD | | | SS-F | | |
|---|---|---|---|---|---|---|---|---|---|---|---|---|---|
| | | Ref. [8] | Ref. [7] | Present | Ref. [8] | Ref. [7] | Present | Ref. [8] | Ref. [7] | Present | Ref. [8] | Ref. [7] | Present |
| 0.1 | 0 | 1.40604 | 1.40652 | 1.40658 | 1.28938 | 1.29186 | 1.29193 | 1.28477 | 1.28514 | 1.28531 | 0.65301 | 0.65269 | 0.65285 |
| | 1 | 1.19765 | 1.19765 | 1.19778 | 1.08942 | 1.09026 | 1.09039 | 1.09009 | 1.09012 | 1.09025 | 0.40173 | 0.40157 | 0.40168 |
| | 2 | 1.10201 | 1.10198 | 1.10209 | 0.97829 | 0.97893 | 0.97905 | 0.97666 | 0.97666 | 0.97676 | 0.27123 | 0.27114 | 0.27122 |
| | 3 | 1.09441 | 1.09447 | 1.09456 | 0.96825 | 0.96920 | 0.96929 | 0.96410 | 0.96418 | 0.96426 | 0.29392 | 0.29405 | 0.29411 |
| | 4 | 1.14855 | 1.14876 | 1.14884 | 1.02961 | 1.03118 | 1.03126 | 1.02428 | 1.02453 | 1.02460 | 0.43106 | 0.43145 | 0.43148 |
| | 5 | 1.25408 | 1.25451 | 1.25457 | 1.14664 | 1.14902 | 1.14909 | 1.14133 | 1.14180 | 1.14186 | 0.61963 | 0.62025 | 0.62027 |
| | 6 | 1.39998 | 1.40065 | 1.40070 | 1.30437 | 1.30763 | 1.30769 | 1.29976 | 1.30048 | 1.30052 | 0.83063 | 0.83145 | 0.83146 |
| | 7 | 1.57477 | 1.57567 | 1.57571 | 1.48943 | 1.49356 | 1.49360 | 1.48582 | 1.48676 | 1.48679 | 1.05216 | 1.05317 | 1.05318 |
| | 8 | 1.76889 | 1.77001 | 1.77004 | 1.69182 | 1.69677 | 1.69680 | 1.68925 | 1.69041 | 1.69044 | 1.27847 | 1.27964 | 1.27965 |
| | 9 | 1.97542 | 1.97675 | 1.97677 | 1.90480 | 1.91050 | 1.91053 | 1.90323 | 1.90459 | 1.90461 | 1.50649 | 1.50782 | 1.50783 |

Table 4: Comparison of the first five frequency parameters $\Omega = \omega R2(\rho h/A11)1/2$ for composite laminated annular plate with different boundary conditions ($R1 = 1$m, $R2 = 3$m, E22 = 10 GPa, E11 = 150 GPa, $\mu 12 = 0.25$, G12 = G13 = 6 GPa, G23 = 5 GPa, $\rho = 1500$ kg/m3, $\varphi = 30^{\circ}$, $h = 0.1$ m).

| Mode | C–C | | | F–C | | | SS-SS | | | SS-C | | |
|---|---|---|---|---|---|---|---|---|---|---|---|---|
| | Ref. [8] | Ref. [10] | Present | Ref. [8] | Ref. [10] | Present | Ref. [8] | Ref. [10] | Present | Ref. [8] | Ref. [10] | Present |
| 1 | 0.41598 | 0.41622 | 0.41634 | 0.11737 | 0.11671 | 0.116727 | 0.21718 | 0.21669 | 0.216753 | 0.32813 | 0.32825 | 0.328328 |
| 2 | 0.41646 | 0.41669 | 0.416811 | 0.14716 | 0.14685 | 0.146861 | 0.21897 | 0.21849 | 0.218557 | 0.32974 | 0.32986 | 0.329938 |
| 3 | 0.4272 | 0.42751 | 0.427631 | 0.24285 | 0.24153 | 0.241557 | 0.23917 | 0.23909 | 0.239146 | 0.34732 | 0.34775 | 0.347824 |
| 4 | 0.46639 | 0.46703 | 0.467137 | 0.36648 | 0.36835 | 0.368394 | 0.30102 | 0.30212 | 0.302167 | 0.40471 | 0.40619 | 0.406262 |
| 5 | 0.54835 | 0.5496 | 0.549691 | 0.49656 | 0.49659 | 0.496707 | 0.40729 | 0.40990 | 0.409954 | 0.51138 | 0.51446 | 0.514521 |
| Mode | SD - SD | | | SD-C | | | SD-SS | | | F-SS | | |
| | Ref. [8] | Ref. [10] | Present | Ref. [8] | Ref. [10] | Present | Ref. [8] | Ref. [10] | Present | Ref. [8] | Ref. [10] | Present |
| 1 | 0.2099 | 0.20933 | 0.209383 | 0.32657 | 0.32666 | 0.326734 | 0.21039 | 0.21192 | 0.21197 | 0.04404 | 0.04255 | 0.042555 |
| 2 | 0.21105 | 0.21045 | 0.210496 | 0.32754 | 0.32759 | 0.32766 | 0.21185 | 0.21218 | 0.212233 | 0.08458 | 0.08408 | 0.084089 |
| 3 | 0.23006 | 0.22978 | 0.22982 | 0.34394 | 0.34422 | 0.344282 | 0.23153 | 0.2313 | 0.231345 | 0.17463 | 0.17302 | 0.173041 |
| 4 | 0.29242 | 0.29332 | 0.293349 | 0.40109 | 0.40239 | 0.402436 | 0.29408 | 0.29579 | 0.295819 | 0.28012 | 0.28132 | 0.281351 |
| 5 | 0.40021 | 0.40270 | 0.402720 | 0.50883 | 0.51178 | 0.511822 | 0.40126 | 0.40619 | 0.406218 | 0.37316 | 0.37312 | 0.373202 |

Table 5: Comparison of the first seven natural frequencies for composite laminated cylindrical shell with variable thickness.

| L/R | | C–C | | | SS-C | | | SS-SS | | |
|---|---|---|---|---|---|---|---|---|---|---|
| | Mode | Present | FEM | Diff, % | Present | FEM | Diff, % | Present | FEM | Diff, % |
| 2 | 1 | 463.621 | 462.27 | 0.29235 | 431.114 | 428.69 | 0.56547 | 411.700 | 411.90 | −0.04860 |
| | 2 | 499.509 | 498.94 | 0.11413 | 465.556 | 462.46 | 0.66948 | 450.037 | 449.28 | 0.16843 |
| | 3 | 583.795 | 582.12 | 0.28775 | 567.576 | 566.67 | 0.15996 | 546.291 | 545.46 | 0.15230 |
| | 4 | 716.031 | 716.37 | -0.04740 | 699.080 | 698.46 | 0.08881 | 691.858 | 691.13 | 0.10532 |
| | 5 | 804.417 | 803.01 | 0.17519 | 799.539 | 798.49 | 0.13140 | 764.667 | 762.36 | 0.30262 |
| | 6 | 849.934 | 847.60 | 0.27534 | 801.679 | 800.09 | 0.19863 | 773.330 | 772.77 | 0.07241 |
| | 7 | 886.213 | 883.37 | 0.32181 | 844.598 | 843.12 | 0.17526 | 807.521 | 805.47 | 0.25458 |
| | 8 | 984.946 | 983.58 | 0.13885 | 942.007 | 940.13 | 0.19968 | 912.805 | 912.27 | 0.05868 |
| | 9 | 994.062 | 995.35 | −0.12940 | 994.062 | 991.67 | 0.24121 | 994.062 | 992.56 | 0.15133 |
| | 10 | 1057.38 | 1054.2 | 0.30202 | 1029.61 | 1025.8 | 0.37156 | 997.300 | 996.15 | 0.11546 |
| 5 | 1 | 200.857 | 199.80 | 0.52880 | 193.204 | 191.05 | 1.12768 | 188.469 | 187.04 | 0.76388 |
| | 2 | 278.030 | 278.79 | −0.27280 | 276.234 | 276.79 | −0.20100 | 270.371 | 271.54 | −0.43070 |
| | 3 | 283.175 | 282.6 | 0.20350 | 278.883 | 277.28 | 0.57828 | 276.385 | 275.32 | 0.38671 |
| | 4 | 370.944 | 371.06 | −0.03140 | 361.981 | 361.36 | 0.17180 | 356.700 | 356.71 | −0.00280 |
| | 5 | 371.760 | 373.63 | -0.50040 | 364.417 | 365.58 | −0.31820 | 358.328 | 360.05 | -0.47830 |
| | 6 | 397.626 | 397.96 | −0.08400 | 397.626 | 397.84 | -0.05380 | 397.626 | 397.74 | -0.02870 |
| | 7 | 448.768 | 454.94 | −1.35680 | 448.739 | 454.91 | −1.35660 | 438.427 | 445.24 | −1.53020 |
| | 8 | 496.636 | 499.18 | −0.50960 | 484.567 | 486.38 | −0.37270 | 475.939 | 478.28 | -0.48950 |
| | 9 | 533.718 | 540.70 | −1.29140 | 532.869 | 539.77 | -1.27850 | 526.072 | 533.28 | −1.35160 |
| | 10 | 560.432 | 560.61 | -0.03180 | 550.341 | 551.33 | −0.17940 | 543.790 | 545.24 | −0.26590 |

In the conical shell, when $\varphi = 30^{\circ}$ or $\varphi = 60^{\circ}$, it is 2340 or 13560. Then, in the annular plate, when R2/R1 = 4 or R2/R1 = 7, it is 2352 or 4640.

Table 6: Comparison of the first ten natural frequencies for laminated composite conical shell with variable thickness and semivertex angles.

| Mode | | C–C | | | SS-C | | | SS-SS | | |
|---|---|---|---|---|---|---|---|---|---|---|
| | | Present | FEM | Diff,% | Present | FEM | Diff,% | Present | FEM | Diff,% |
| $\varphi = 30^{\circ}$ | 1 | 106.993 | 107.59 | -0.5544 | 105.248 | 105.54 | −0.2764 | 101.277 | 102.25 | −0.9513 |
| | 2 | 109.593 | 109.67 | −0.0704 | 109.418 | 109.44 | -0.0205 | 103.802 | 104.25 | −0.4302 |
| | 3 | 122.583 | 122.61 | −0.0217 | 122.570 | 122.59 | −0.0163 | 114.849 | 115.70 | −0.7352 |
| | 4 | 133.667 | 134.40 | −0.5451 | 130.664 | 130.87 | −0.1577 | 127.989 | 128.74 | −0.5831 |
| | 5 | 141.705 | 141.98 | −0.1935 | 141.703 | 141.97 | −0.1882 | 131.646 | 132.75 | −0.8320 |
| | 6 | 165.960 | 166.65 | −0.4141 | 165.959 | 166.65 | −0.4144 | 153.575 | 155.04 | −0.9451 |
| | 7 | 192.770 | 193.1 | -0.1709 | 192.232 | 192.47 | -0.1234 | 180.162 | 182.14 | −1.0861 |
| | 8 | 194.714 | 196.02 | -0.6661 | 194.714 | 196.02 | -0.6662 | 187.516 | 188.04 | -0.2786 |
| | 9 | 201.544 | 201.88 | -0.1664 | 198.360 | 198.31 | 0.0254 | 195.297 | 195.50 | -0.1039 |
| | 10 | 205.172 | 205.57 | -0.1937 | 205.145 | 205.53 | -0.1871 | 198.028 | 198.71 | -0.3433 |
| $\varphi = 60^{\circ}$ | 1 | 64.1424 | 64.046 | 0.15055 | 63.9952 | 63.849 | 0.2289 | 58.9974 | 59.459 | −0.7763 |
| | 2 | 65.2568 | 65.344 | −0.13350 | 64.1582 | 64.007 | 0.2362 | 60.6757 | 61.061 | −0.6311 |
| | 3 | 70.0279 | 69.844 | 0.26330 | 70.0125 | 69.821 | 0.2743 | 63.3633 | 63.797 | −0.6798 |
| | 4 | 79.7110 | 79.525 | 0.23388 | 79.7072 | 79.520 | 0.2354 | 71.4290 | 71.838 | -0.5693 |
| | 5 | 83.6041 | 83.637 | −0.03930 | 81.4993 | 81.162 | 0.4155 | 79.3319 | 79.378 | -0.0581 |
| | 6 | 92.1487 | 92.016 | 0.14420 | 92.1473 | 92.014 | 0.1449 | 82.3620 | 82.763 | −0.4845 |
| | 7 | 106.772 | 106.74 | 0.03003 | 106.772 | 106.74 | 0.0296 | 95.6238 | 96.052 | -0.4459 |
| | 8 | 121.047 | 120.90 | 0.12177 | 120.632 | 120.41 | 0.1840 | 110.851 | 111.36 | -0.4573 |
| | 9 | 123.238 | 123.38 | -0.11490 | 123.238 | 123.24 | -0.0016 | 114.694 | 114.67 | 0.0213 |
| | 10 | 125.638 | 125.28 | 0.28616 | 123.555 | 123.38 | 0.1418 | 119.320 | 119.18 | 0.1176 |

Table 7: Comparison of the first ten natural frequencies for laminated composite annular plate with variable thickness and radius ratio R2/R1.

| | | C–C | | | F–C | | | SS-SS | | | SS-C | | |
|---|---|---|---|---|---|---|---|---|---|---|---|---|---|
| R2/R1 | Mode | Present | FEM | Diff, % | Present | FEM | Diff, % | Present | FEM | Diff, % | Present | FEM | Diff, % |
| 4 | 1 | 80.8330 | 80.913 | −0.098 | 22.8862 | 22.880 | 0.027 | 53.3540 | 53.322 | 0.060 | 66.1815 | 66.204 | −0.033 |
| | 2 | 82.2978 | 82.246 | 0.062 | 34.8074 | 34.903 | −0.273 | 57.0347 | 57.072 | −0.065 | 68.4974 | 68.639 | −0.206 |
| | 3 | 85.4462 | 85.413 | 0.038 | 58.0420 | 57.861 | 0.313 | 57.7302 | 57.279 | 0.788 | 70.5978 | 70.223 | 0.534 |
| | 4 | 95.5326 | 95.267 | 0.279 | 86.8110 | 86.638 | 0.200 | 75.2113 | 74.614 | 0.801 | 89.4533 | 89.033 | 0.472 |
| | 5 | 120.276 | 119.99 | 0.238 | 106.909 | 107.33 | −0.392 | 101.282 | 100.90 | 0.379 | 118.520 | 118.57 | −0.042 |
| | 6 | 152.148 | 152.05 | 0.064 | 110.360 | 111.36 | −0.897 | 131.460 | 131.42 | 0.030 | 151.851 | 152.50 | −0.425 |
| | 7 | 188.011 | 188.26 | -0.132 | 118.282 | 118.43 | −0.124 | 154.411 | 155.88 | −0.942 | 187.974 | 189.41 | −0.758 |
| | 8 | 219.814 | 220.85 | −0.469 | 146.850 | 148.28 | −0.964 | 158.098 | 159.20 | −0.692 | 192.220 | 193.47 | −0.646 |
| | 9 | 220.975 | 222.05 | −0.484 | 151.800 | 152.47 | −0.439 | 161.851 | 163.02 | −0.717 | 196.075 | 198.04 | −0.992 |
| | 10 | 223.295 | 224.15 | −0.381 | 187.928 | 189.37 | −0.761 | 164.766 | 165.31 | −0.329 | 196.198 | 198.04 | −0.93 |
| 7 | 1 | 20.4157 | 20.411 | 0.023 | 6.90231 | 6.8513 | 0.745 | 13.7631 | 13.685 | 0.570 | 17.6432 | 17.547 | 0.548 |
| | 2 | 21.8238 | 21.733 | 0.418 | 11.9496 | 11.872 | 0.654 | 15.9658 | 15.904 | 0.388 | 19.2642 | 19.212 | 0.272 |
| | 3 | 22.8519 | 22.808 | 0.192 | 19.2561 | 19.106 | 0.786 | 16.2534 | 16.153 | 0.622 | 20.2551 | 20.058 | 0.983 |
| | 4 | 28.6074 | 28.517 | 0.317 | 28.3381 | 28.257 | 0.287 | 23.4271 | 23.253 | 0.749 | 28.3576 | 28.263 | 0.335 |
| | 5 | 38.0339 | 38.098 | −0.168 | 30.7778 | 30.750 | 0.090 | 32.1193 | 32.039 | 0.250 | 38.0205 | 38.089 | −0.180 |
| | 6 | 48.6514 | 48.991 | −0.693 | 36.6121 | 36.776 | −0.445 | 41.0108 | 41.240 | −0.556 | 48.6505 | 48.990 | −0.692 |
| | 7 | 56.7257 | 57.108 | −0.669 | 38.0076 | 38.075 | −0.177 | 41.8625 | 41.997 | −0.320 | 51.0011 | 51.398 | −0.772 |
| | 8 | 57.9807 | 58.205 | −0.385 | 48.6433 | 48.984 | −0.695 | 43.7549 | 43.873 | −0.269 | 53.2509 | 53.609 | −0.667 |
| | 9 | 59.3585 | 59.937 | −0.965 | 49.5905 | 49.859 | −0.538 | 44.4490 | 44.561 | −0.251 | 53.7503 | 54.023 | −0.504 |
| | 10 | 60.3139 | 60.905 | −0.970 | 60.3111 | 60.903 | −0.971 | 52.6400 | 53.162 | −0.982 | 60.3136 | 60.805 | −0.808 |

boundary condition. Then, regardless of the cylindrical shell with even thickness, the frequency parameters of the cylindrical shell with varying thickness have different values in the opposite boundary conditions (C–F and F–C). It is because of the changes in the boundary condition caused by different thicknesses.

Then, the effect of $\alpha$ and $\lambda$ on the frequency parameter is investigated. Figure 6 shows the change of the frequency parameter ($n = 2$, $m = 1$) of the laminated composite structures according to the changes of $\alpha$ and $\lambda$. The material properties and geometric dimensions are the same as Table 8–10. In Figure 6, when $\lambda$ increases, the frequency parameter converges to a certain value.

Figure 7 presents the variation of frequency parameters of the laminated composite conical shell, cylindrical shell, and annular plate with variable thickness according to different circumferential wave number $n$. The material properties are E11/$E22 = 15$ and $\phi$f = [90°/0°/90°/0°], and the parameter for

Table 8: The frequency parameters for laminated composite conical shell with variable thickness and different boundary conditions.

| | | BCs | | | | | | | | | | | | |
|---|---|---|---|---|---|---|---|---|---|---|---|---|---|---|
| n | m | C–C | C–F | F–C | SS-SS | C-SS | SD - SD | C-SD | EI-C | EII-C | EIII-C | EI-EI | EII-EII | EIII-EIII |
| | 1 | 0.62 | 0.234 | 0.47 | 0.588 | 0.601 | 0.435 | 0.599 | 0.53 | 0.619 | 0.529 | 0.41 | 0.619 | 0.409 |
| | 2 | 0.996 | 0.721 | 0.843 | 0.895 | 0.92 | 0.761 | 0.914 | 0.897 | 0.994 | 0.897 | 0.41 | 0.993 | 0.409 |
| 1 | 3 | 1.43 | 1.012 | 1.146 | 1.259 | 1.323 | 0.89 | 1.323 | 1.238 | 1.424 | 1.238 | 0.861 | 1.422 | 0.86 |
| | 4 | 1.972 | 1.387 | 1.537 | 1.777 | 1.875 | 1.266 | 1.788 | 1.684 | 1.971 | 1.683 | 1.165 | 1.97 | 1.164 |
| | 5 | 2.034 | 1.466 | 1.803 | 1.982 | 1.993 | 1.775 | 1.901 | 1.832 | 2.024 | 1.832 | 1.504 | 2.022 | 1.504 |
| | 1 | 0.434 | 0.153 | 0.283 | 0.383 | 0.411 | 0.385 | 0.41 | 0.381 | 0.432 | 0.379 | 0.301 | 0.432 | 0.299 |
| | 2 | 0.852 | 0.555 | 0.612 | 0.731 | 0.78 | 0.725 | 0.776 | 0.732 | 0.847 | 0.731 | 0.546 | 0.846 | 0.545 |
| 2 | 3 | 1.343 | 0.898 | 0.972 | 1.146 | 1.23 | 0.95 | 1.23 | 1.114 | 1.335 | 1.113 | 0.865 | 1.333 | 0.864 |
| | 4 | 1.967 | 1.378 | 1.437 | 1.71 | 1.825 | 1.159 | 1.823 | 1.608 | 1.954 | 1.606 | 1.056 | 1.952 | 1.054 |
| | 5 | 2.713 | 2.01 | 2.055 | 2.421 | 2.552 | 1.709 | 2.288 | 2.247 | 2.697 | 2.242 | 1.438 | 2.693 | 1.437 |
| | 1 | 0.352 | 0.121 | 0.206 | 0.287 | 0.322 | 0.285 | 0.318 | 0.321 | 0.349 | 0.319 | 0.283 | 0.349 | 0.28 |
| | 2 | 0.762 | 0.449 | 0.479 | 0.623 | 0.688 | 0.621 | 0.685 | 0.655 | 0.757 | 0.653 | 0.576 | 0.756 | 0.574 |
| 3 | 3 | 1.281 | 0.822 | 0.861 | 1.07 | 1.166 | 1.067 | 1.166 | 1.048 | 1.272 | 1.047 | 0.949 | 1.27 | 0.948 |
| | 4 | 1.927 | 1.324 | 1.365 | 1.661 | 1.782 | 1.404 | 1.781 | 1.559 | 1.913 | 1.557 | 1.235 | 1.91 | 1.233 |
| | 5 | 2.688 | 1.974 | 2.015 | 2.39 | 2.525 | 1.66 | 2.525 | 2.22 | 2.671 | 2.214 | 1.45 | 2.667 | 1.449 |
| | 1 | 0.316 | 0.109 | 0.202 | 0.246 | 0.28 | 0.24 | 0.274 | 0.298 | 0.314 | 0.296 | 0.275 | 0.313 | 0.273 |
| | 2 | 0.716 | 0.392 | 0.428 | 0.567 | 0.637 | 0.566 | 0.636 | 0.632 | 0.71 | 0.629 | 0.583 | 0.709 | 0.579 |
| 4 | 3 | 1.246 | 0.776 | 0.807 | 1.026 | 1.128 | 1.026 | 1.128 | 1.032 | 1.236 | 1.03 | 0.947 | 1.234 | 0.944 |
| | 4 | 1.902 | 1.292 | 1.327 | 1.632 | 1.757 | 1.631 | 1.756 | 1.545 | 1.889 | 1.543 | 1.337 | 1.886 | 1.335 |
| | 5 | 2.672 | 1.953 | 1.992 | 2.371 | 2.508 | 1.864 | 2.508 | 2.21 | 2.655 | 2.205 | 1.782 | 2.651 | 1.781 |
| | 1 | 0.308 | 0.113 | 0.24 | 0.24 | 0.267 | 0.232 | 0.26 | 0.298 | 0.306 | 0.296 | 0.281 | 0.306 | 0.279 |
| | 2 | 0.698 | 0.368 | 0.444 | 0.548 | 0.616 | 0.548 | 0.615 | 0.638 | 0.693 | 0.634 | 0.597 | 0.691 | 0.593 |
| 5 | 3 | 1.231 | 0.755 | 0.798 | 1.009 | 1.112 | 1.009 | 1.112 | 1.049 | 1.221 | 1.046 | 0.965 | 1.219 | 0.961 |
| | 4 | 1.893 | 1.279 | 1.318 | 1.621 | 1.746 | 1.62 | 1.746 | 1.559 | 1.879 | 1.557 | 1.365 | 1.876 | 1.363 |
| | 5 | 2.666 | 1.945 | 1.987 | 2.365 | 2.502 | 2.321 | 2.502 | 2.22 | 2.65 | 2.214 | 1.888 | 2.646 | 1.884 |

Table 9: The frequency parameters for laminated composite cylindrical shell with variable thickness and different boundary conditions.

| | | BCs | | | | | | | | | | | | |
|---|---|---|---|---|---|---|---|---|---|---|---|---|---|---|
| n | m | C–C | C–F | F–C | SS-SS | C-SS | SD - SD | C-SD | EI-C | EII-C | EIII-C | EI-EI | EII-EII | EIII-EIII |
| | 1 | 0.854 | 0.496 | 0.353 | 0.829 | 0.847 | 0.806 | 0.841 | 0.551 | 0.852 | 0.55 | 0.437 | 0.852 | 0.436 |
| | 2 | 1.591 | 1.238 | 1.17 | 1.53 | 1.569 | 0.806 | 1.569 | 1.255 | 1.587 | 1.255 | 0.651 | 1.587 | 0.651 |
| 1 | 3 | 2.173 | 1.851 | 1.798 | 2.061 | 2.12 | 1.53 | 2.12 | 1.878 | 2.167 | 1.878 | 1.202 | 2.166 | 1.202 |
| | 4 | 2.72 | 2.308 | 2.252 | 2.547 | 2.63 | 2.061 | 2.63 | 2.32 | 2.711 | 2.32 | 1.689 | 2.709 | 1.689 |
| | 5 | 3.342 | 2.8 | 2.334 | 3.122 | 3.226 | 2.547 | 2.973 | 2.429 | 3.331 | 2.428 | 2.204 | 3.328 | 2.203 |
| | 1 | 0.584 | 0.329 | 0.196 | 0.537 | 0.569 | 0.53 | 0.556 | 0.448 | 0.582 | 0.446 | 0.399 | 0.581 | 0.398 |
| | 2 | 1.163 | 0.831 | 0.75 | 1.066 | 1.125 | 1.066 | 1.126 | 0.896 | 1.157 | 0.895 | 0.706 | 1.157 | 0.705 |
| 2 | 3 | 1.759 | 1.384 | 1.318 | 1.61 | 1.692 | 1.55 | 1.692 | 1.438 | 1.751 | 1.438 | 1.275 | 1.75 | 1.274 |
| | 4 | 2.403 | 1.92 | 1.865 | 2.199 | 2.302 | 1.607 | 2.302 | 2.005 | 2.391 | 2.003 | 1.487 | 2.389 | 1.486 |
| | 5 | 3.124 | 2.522 | 2.486 | 2.877 | 2.996 | 2.199 | 2.996 | 2.612 | 3.11 | 2.609 | 1.879 | 3.107 | 1.879 |
| | 1 | 0.464 | 0.26 | 0.157 | 0.405 | 0.442 | 0.387 | 0.426 | 0.402 | 0.461 | 0.4 | 0.372 | 0.461 | 0.369 |
| | 2 | 0.957 | 0.631 | 0.554 | 0.835 | 0.906 | 0.834 | 0.906 | 0.766 | 0.951 | 0.765 | 0.686 | 0.95 | 0.683 |
| 3 | 3 | 1.538 | 1.133 | 1.066 | 1.358 | 1.456 | 1.357 | 1.455 | 1.234 | 1.528 | 1.234 | 1.113 | 1.527 | 1.111 |
| | 4 | 2.206 | 1.68 | 1.624 | 1.975 | 2.094 | 1.975 | 2.094 | 1.798 | 2.193 | 1.795 | 1.54 | 2.19 | 1.539 |
| | 5 | 2.965 | 2.327 | 2.293 | 2.699 | 2.83 | 2.324 | 2.83 | 2.482 | 2.949 | 2.476 | 2.154 | 2.946 | 2.15 |
| | 1 | 0.432 | 0.26 | 0.237 | 0.373 | 0.406 | 0.352 | 0.391 | 0.401 | 0.43 | 0.399 | 0.379 | 0.429 | 0.376 |
| | 2 | 0.868 | 0.549 | 0.489 | 0.733 | 0.808 | 0.731 | 0.808 | 0.742 | 0.862 | 0.739 | 0.692 | 0.861 | 0.688 |
| 4 | 3 | 1.432 | 1.008 | 0.95 | 1.234 | 1.339 | 1.233 | 1.339 | 1.166 | 1.422 | 1.165 | 1.067 | 1.42 | 1.065 |
| | 4 | 2.104 | 1.554 | 1.504 | 1.857 | 1.983 | 1.857 | 1.983 | 1.709 | 2.09 | 1.706 | 1.493 | 2.088 | 1.491 |
| | 5 | 2.876 | 2.217 | 2.186 | 2.597 | 2.735 | 2.597 | 2.735 | 2.395 | 2.86 | 2.389 | 2.069 | 2.856 | 2.065 |
| | 1 | 0.47 | 0.316 | 0.37 | 0.419 | 0.442 | 0.402 | 0.43 | 0.454 | 0.468 | 0.452 | 0.436 | 0.468 | 0.434 |
| | 2 | 0.855 | 0.552 | 0.523 | 0.72 | 0.791 | 0.717 | 0.79 | 0.774 | 0.849 | 0.77 | 0.732 | 0.848 | 0.728 |
| 5 | 3 | 1.398 | 0.968 | 0.925 | 1.193 | 1.3 | 1.192 | 1.299 | 1.178 | 1.388 | 1.176 | 1.09 | 1.386 | 1.087 |
| | 4 | 2.065 | 1.505 | 1.465 | 1.811 | 1.94 | 1.81 | 1.94 | 1.698 | 2.051 | 1.695 | 1.506 | 2.049 | 1.504 |
| | 5 | 2.84 | 2.171 | 2.145 | 2.555 | 2.695 | 2.554 | 2.695 | 2.372 | 2.823 | 2.366 | 2.055 | 2.819 | 2.051 |

Table 10: The frequency parameters for laminated composite annular plate with variable thickness and different boundary conditions.

| | | BCs | | | | | | | | | | | | |
|---|---|---|---|---|---|---|---|---|---|---|---|---|---|---|
| n | m | C–C | C–F | F–C | SS-SS | C-SS | SD - SD | C-SD | EI-C | EII-C | EIII-C | EI-EI | EII-EII | EIII-EIII |
| 1 | 1 | 0.211 | 0.04 | 0.043 | 0.101 | 0.153 | 0.101 | 0.153 | 0.199 | 0.208 | 0.197 | 0.196 | 0.208 | 0.193 |
| | 2 | 0.579 | 0.226 | 0.22 | 0.392 | 0.482 | 0.392 | 0.482 | 0.489 | 0.573 | 0.486 | 0.389 | 0.572 | 0.389 |
| | 3 | 1.111 | 0.603 | 0.602 | 0.861 | 0.981 | 0.832 | 0.981 | 0.854 | 1.1 | 0.854 | 0.471 | 1.098 | 0.468 |
| | 4 | 1.676 | 0.957 | 1.15 | 1.487 | 1.626 | 0.861 | 1.541 | 1.377 | 1.676 | 1.374 | 0.797 | 1.676 | 0.796 |
| | 5 | 1.78 | 1.142 | 1.462 | 1.676 | 1.676 | 1.487 | 1.626 | 1.483 | 1.765 | 1.483 | 1.208 | 1.762 | 1.206 |
| 2 | 1 | 0.213 | 0.041 | 0.069 | 0.105 | 0.155 | 0.105 | 0.155 | 0.202 | 0.21 | 0.2 | 0.198 | 0.21 | 0.196 |
| | 2 | 0.582 | 0.228 | 0.236 | 0.396 | 0.485 | 0.396 | 0.485 | 0.499 | 0.575 | 0.496 | 0.48 | 0.574 | 0.477 |
| | 3 | 1.114 | 0.606 | 0.612 | 0.865 | 0.984 | 0.865 | 0.984 | 0.87 | 1.103 | 0.87 | 0.573 | 1.101 | 0.573 |
| | 4 | 1.783 | 1.145 | 1.158 | 1.491 | 1.629 | 0.886 | 1.629 | 1.389 | 1.768 | 1.387 | 0.812 | 1.765 | 0.81 |
| | 5 | 2.538 | 1.719 | 1.849 | 2.25 | 2.396 | 1.491 | 2.01 | 2.075 | 2.538 | 2.069 | 1.22 | 2.538 | 1.218 |
| 3 | 1 | 0.217 | 0.044 | 0.105 | 0.114 | 0.159 | 0.114 | 0.159 | 0.207 | 0.215 | 0.205 | 0.204 | 0.214 | 0.201 |
| | 2 | 0.587 | 0.233 | 0.267 | 0.404 | 0.49 | 0.404 | 0.49 | 0.515 | 0.58 | 0.511 | 0.494 | 0.579 | 0.49 |
| | 3 | 1.119 | 0.611 | 0.63 | 0.872 | 0.989 | 0.872 | 0.989 | 0.897 | 1.108 | 0.895 | 0.835 | 1.106 | 0.832 |
| | 4 | 1.788 | 1.151 | 1.171 | 1.498 | 1.634 | 1.204 | 1.634 | 1.411 | 1.773 | 1.408 | 1.014 | 1.77 | 1.014 |
| | 5 | 2.57 | 1.831 | 1.86 | 2.256 | 2.401 | 1.498 | 2.293 | 2.091 | 2.553 | 2.085 | 1.24 | 2.549 | 1.238 |
| 4 | 1 | 0.225 | 0.052 | 0.146 | 0.13 | 0.167 | 0.13 | 0.167 | 0.217 | 0.223 | 0.215 | 0.213 | 0.222 | 0.211 |
| | 2 | 0.595 | 0.242 | 0.316 | 0.417 | 0.498 | 0.417 | 0.498 | 0.535 | 0.589 | 0.532 | 0.513 | 0.587 | 0.509 |
| | 3 | 1.127 | 0.62 | 0.658 | 0.884 | 0.998 | 0.884 | 0.998 | 0.932 | 1.116 | 0.93 | 0.865 | 1.114 | 0.862 |
| | 4 | 1.796 | 1.159 | 1.191 | 1.508 | 1.642 | 1.508 | 1.642 | 1.442 | 1.781 | 1.44 | 1.269 | 1.778 | 1.267 |
| | 5 | 2.578 | 1.839 | 1.876 | 2.266 | 2.409 | 1.589 | 2.409 | 2.114 | 2.56 | 2.108 | 1.463 | 2.556 | 1.463 |
| 5 | 1 | 0.239 | 0.063 | 0.186 | 0.153 | 0.181 | 0.153 | 0.181 | 0.233 | 0.237 | 0.231 | 0.229 | 0.236 | 0.227 |
| | 2 | 0.608 | 0.257 | 0.383 | 0.438 | 0.512 | 0.438 | 0.512 | 0.561 | 0.602 | 0.557 | 0.536 | 0.601 | 0.532 |
| | 3 | 1.139 | 0.634 | 0.701 | 0.901 | 1.01 | 0.901 | 1.01 | 0.975 | 1.129 | 0.971 | 0.902 | 1.126 | 0.898 |
| | 4 | 1.807 | 1.172 | 1.219 | 1.523 | 1.654 | 1.523 | 1.654 | 1.484 | 1.793 | 1.481 | 1.307 | 1.79 | 1.305 |
| | 5 | 2.588 | 1.851 | 1.898 | 2.279 | 2.42 | 1.983 | 2.42 | 2.145 | 2.571 | 2.139 | 1.815 | 2.567 | 1.812 |

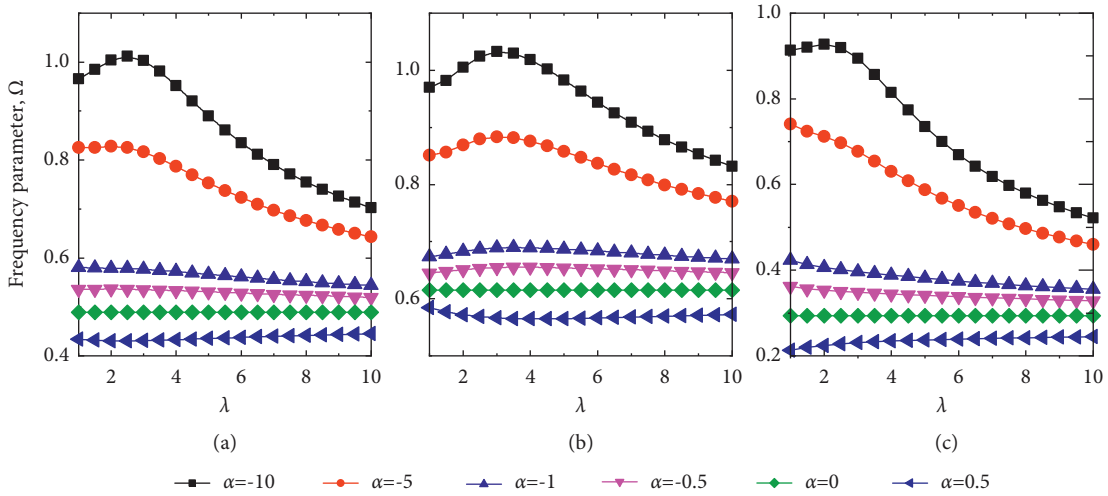


Figure 6: Frequency parameters of laminated composite structures according to the change of thickness variation parameter $\alpha$ and $\lambda$, (a) conical shell, (b) cylindrical shell, and (c) annular plate.

thickness profile is $\lambda = 1$. The geometric dimensions are $R = 1$m, $L = 2$m, $h1 = 0.1$ m in the cylindrical shell, $R1 = 1$m, $L = 2$m, $\varphi = 30^{\circ}$, $h1 = 0.1$ m in the conical shell, and $R1 = 1$m, $R2 = 3$m, $h1 = 0.1$ m in the annular plate. In Figure 7, regardless of the laminated composite structures, the frequency parameter first increases, and then decreases according to the increase of circumferential wave number. In C–C and SS-SS boundary, the frequency parameter in $\alpha = -0.5$ is more than that in $\alpha = 0$. The value in $\alpha = 0.5$ is less than that in $\alpha = 0$. In a C–F boundary condition, the value in $\alpha = -0.5$ is less than that in $\alpha = 0$ at the start point. However, when the circumferential wave number reaches a certain value, the value increases again. In addition, the value in $\alpha = 0.5$ is more than that in $\alpha = 0$ at start point. However, when the circumferential wave number reaches a certain value, the value decreases again. In EI-EI boundary condition, the value changes irregularly at the start point. However, when the circumferential wave number exceeds a certain value, the value increases.

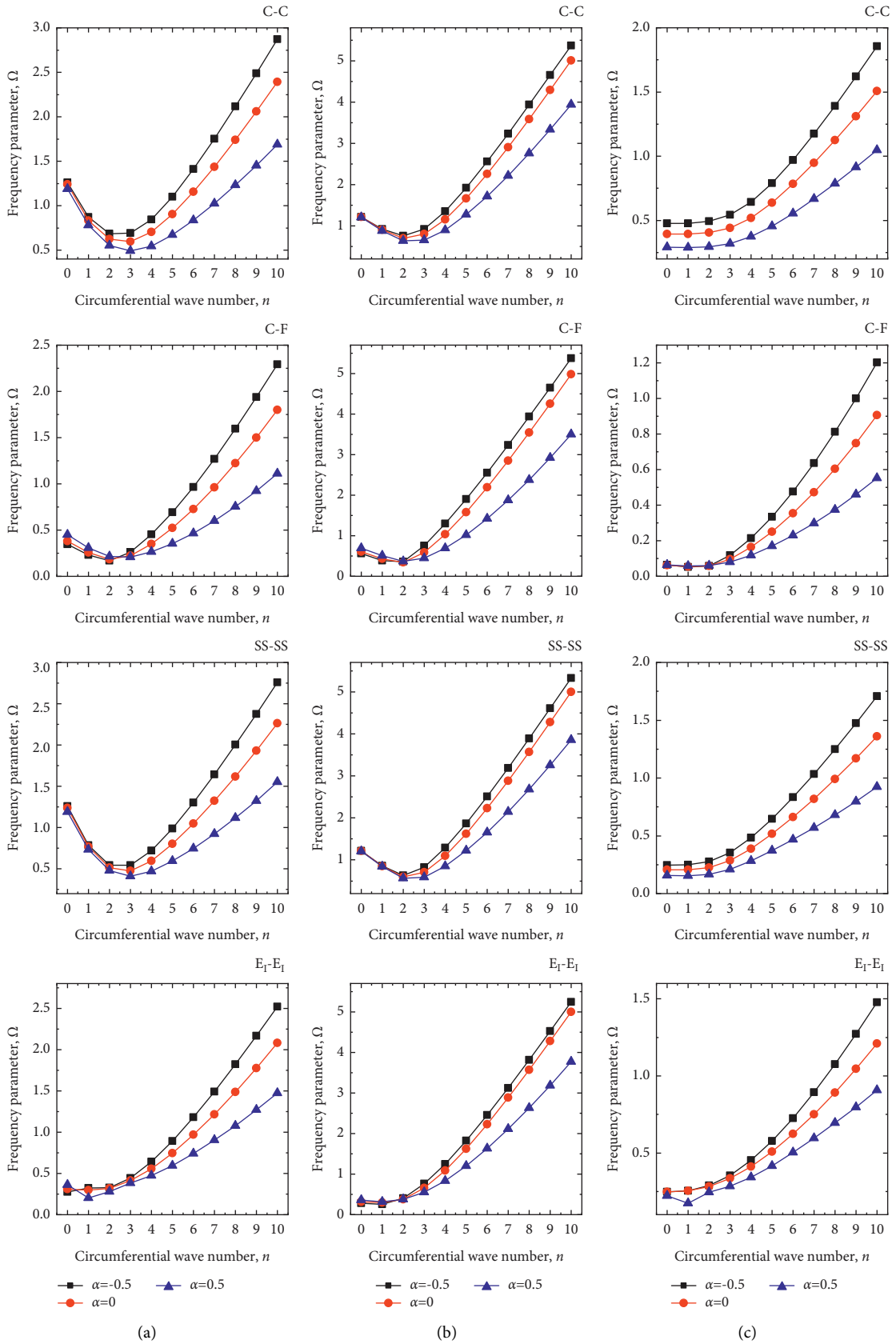


FIGURE 7: Variation of frequency parameters of laminated composite structures with different circumferential wave number and variable thickness ($m = 1$), (a) conical shell, (b) cylindrical shell, and (c) annular plate.

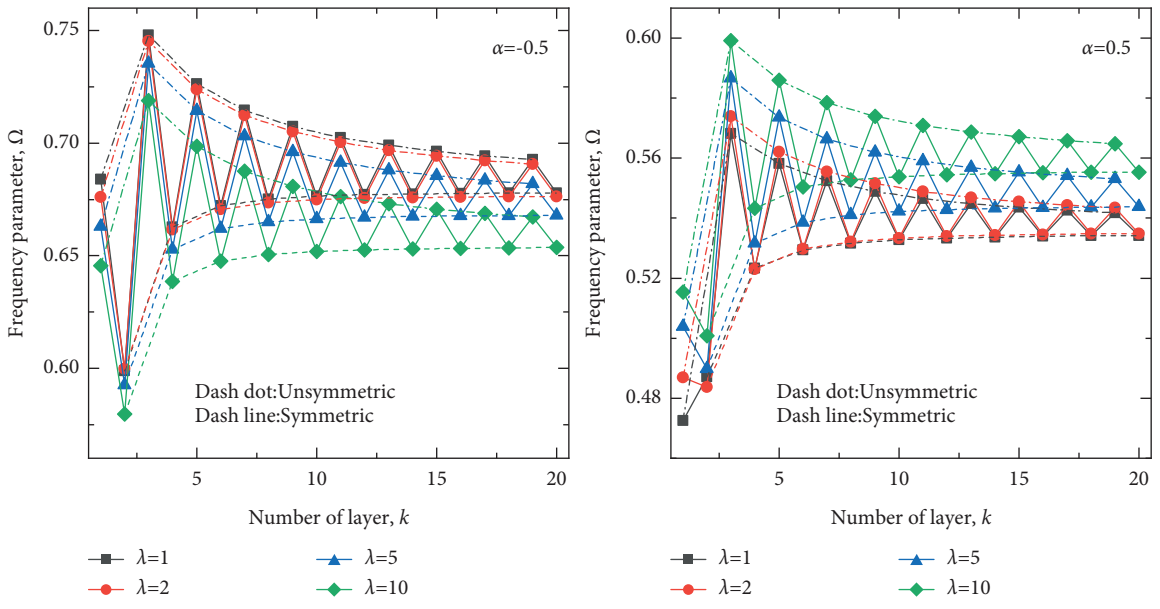


(a)

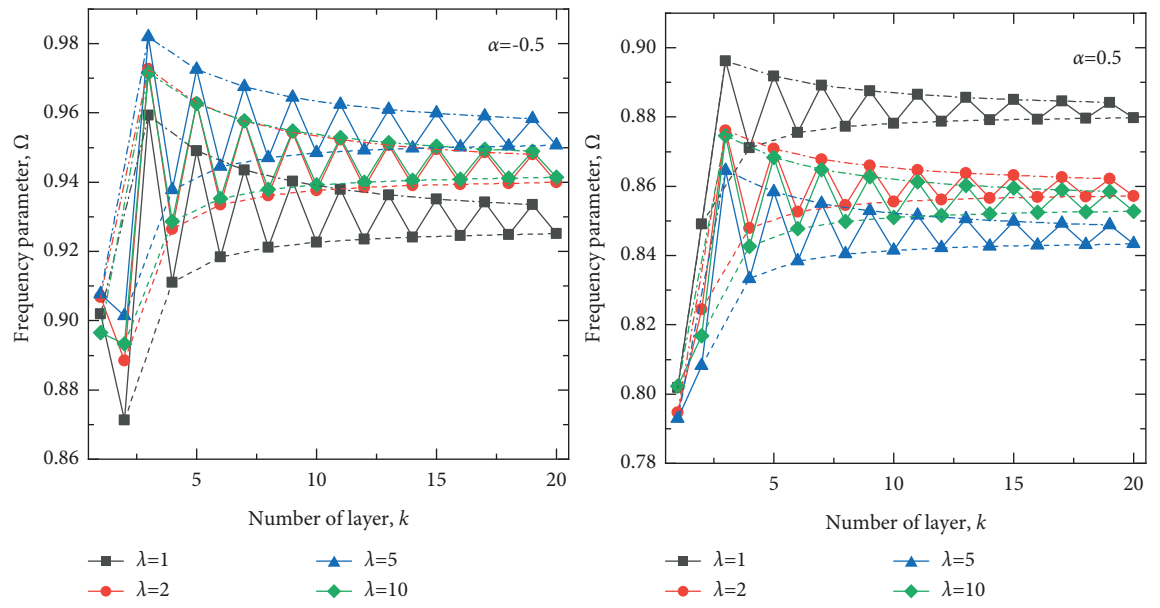


(b)

Figure 8: Continued.

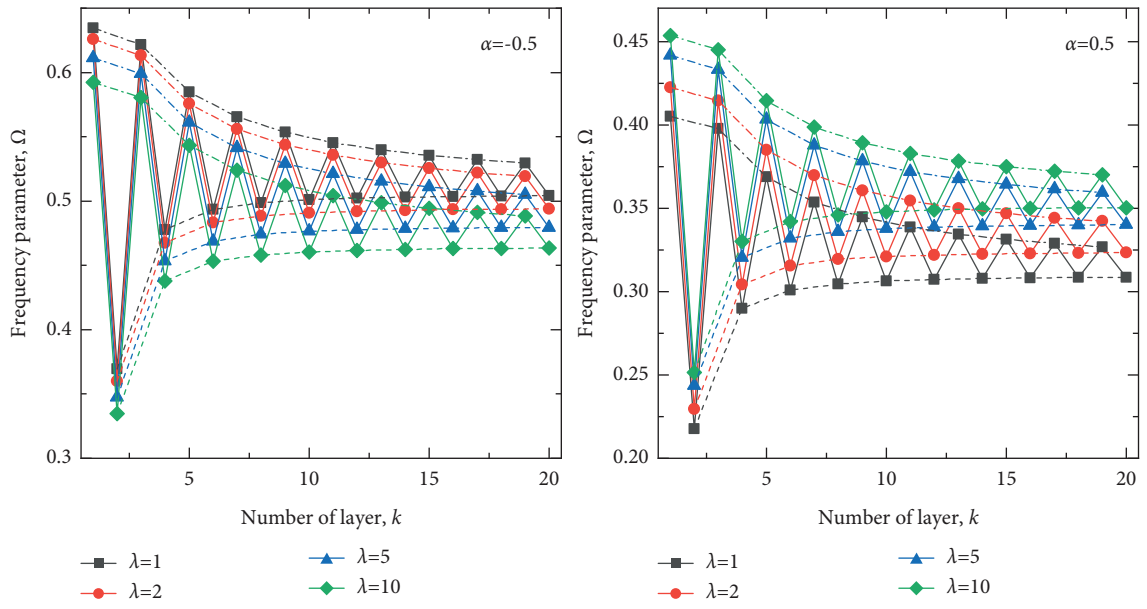


(c)

Figure 8: Variation of the frequency parameter according to lamina number k for [0°/90°]k laminated composite structures with C–C boundary condition and variable thickness($n = 1$, $m = 1$): (a) conical shell, (b) cylindrical shell, and (c) annular plate.

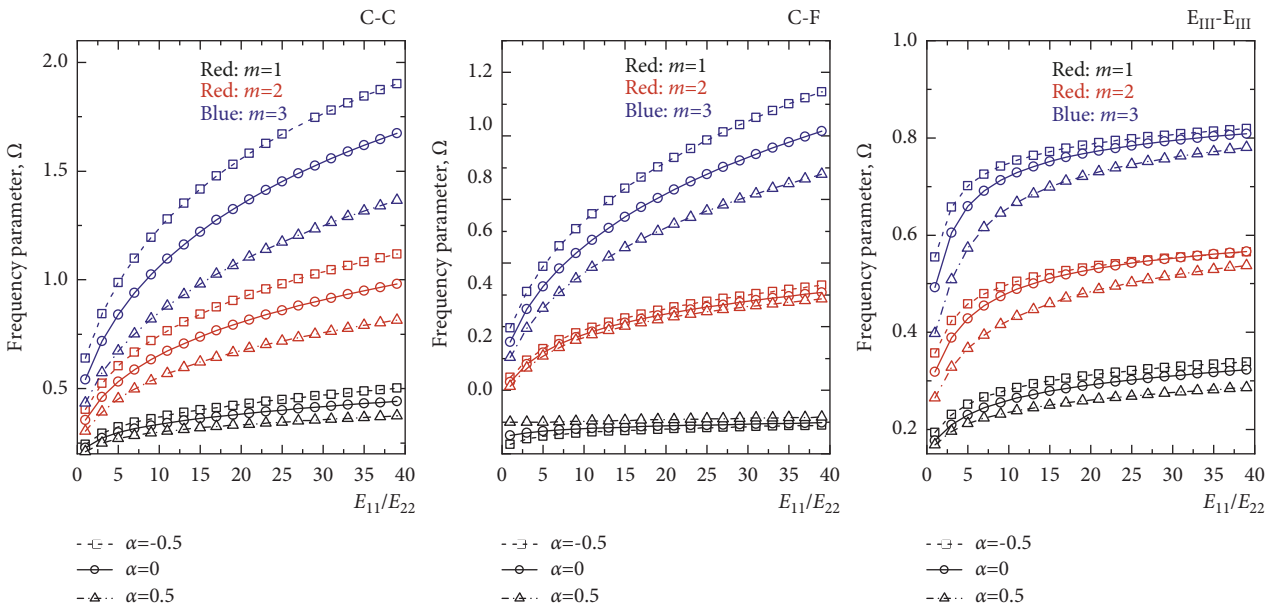


(a)

Figure 9: Continued.

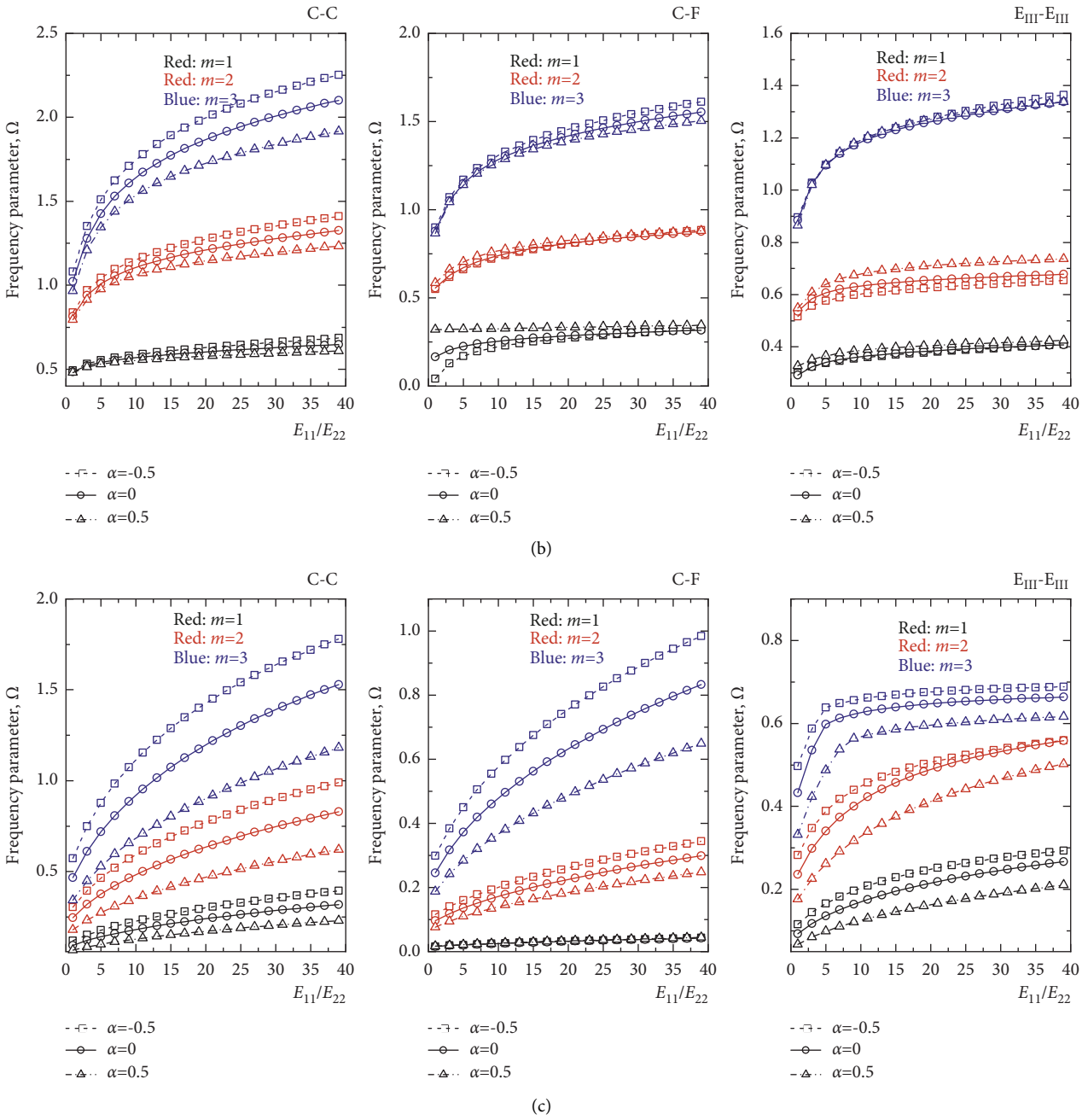


FIGURE 9: The frequency parameters of the laminated composite structures with different stiffness ratios and variable thickness ($n = 2$): (a) conical shell, (b) cylindrical shell, and (c) annular plate.

As the next example, the effect of the number of layers on the free vibration of laminated composite structures with C–C boundary condition will be investigated. The material properties are E11/$E22 = 15$, and the geometric dimensions are $R = 1$m, $L = 2$m, $h1 = 0.1$ m in the cylindrical shell, $R1 = 1$m, $L = 2$m, $\varphi = 60^{\circ}$, $h1 = 0.1$ m in the conical shell, and $R1 = 1$m, $R2 = 3$m, $h1 = 0.1$ m in the annular plate.

In Figure 8, the variations of the frequency parameters for the laminated composite structures with [0°/90°]k layouts (where $k$ denotes the number of layer of the composite structures, and $k = 1$ means for the single-layered schemes [0°], $k = 2$ for two-layered [0°/90°] unsymmetric schemes, $k = 3$ for three-layered [0°/90°/0] symmetric ones, and so on) according to the number of layers $k$ are depicted. It is clearly shown from Figure 8 that, for the unsymmetric scheme, as the number of layers increases, the frequency parameters of laminated composite structures increase rapidly until the number of layers is larger than six. Another observation is that, for the unsymmetric schemes, the frequency parameters are always larger than those of the symmetric ones.

In the last example, Figure 9 shows the variations of the first three frequency parameters of [0°/90°/0°/90°] laminated composite structures with variable thickness according to the elastic modulus ratios. The material properties and

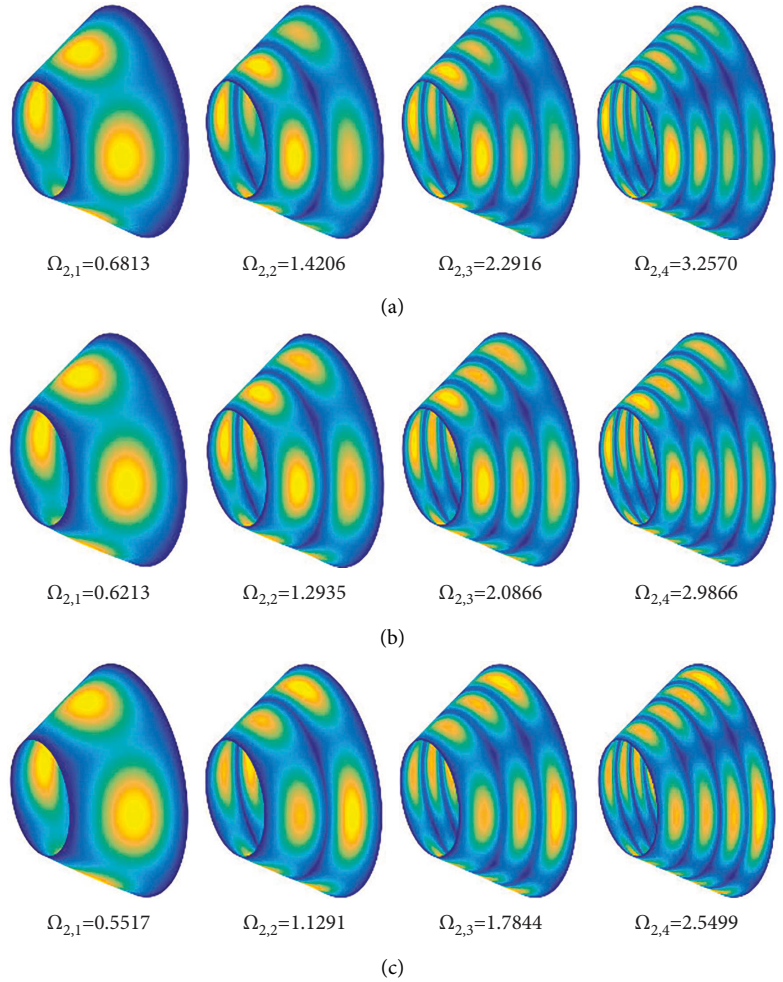


Figure 10: Mode shapes of laminated composite conical shell with variable thickness, (a) $\alpha = -0.5$, (b) $\alpha = 0$, and (c) $\alpha = 0.5$.

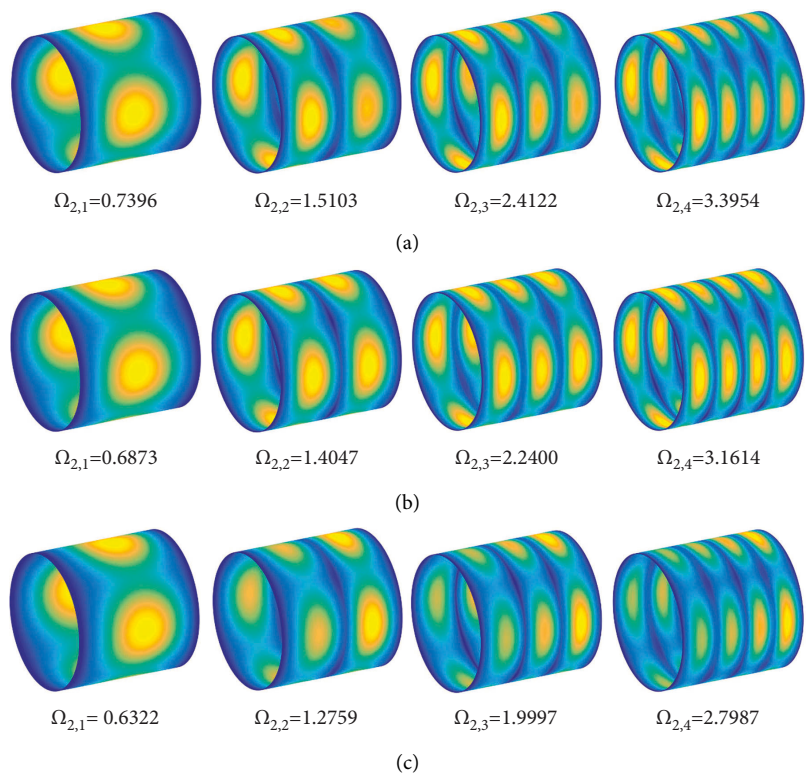


Figure 11: Mode shapes of laminated composite cylindrical shell with variable thickness, (a) $\alpha = -0.5$, (b) $\alpha = 0$, and (c) $\alpha = 0.5$.

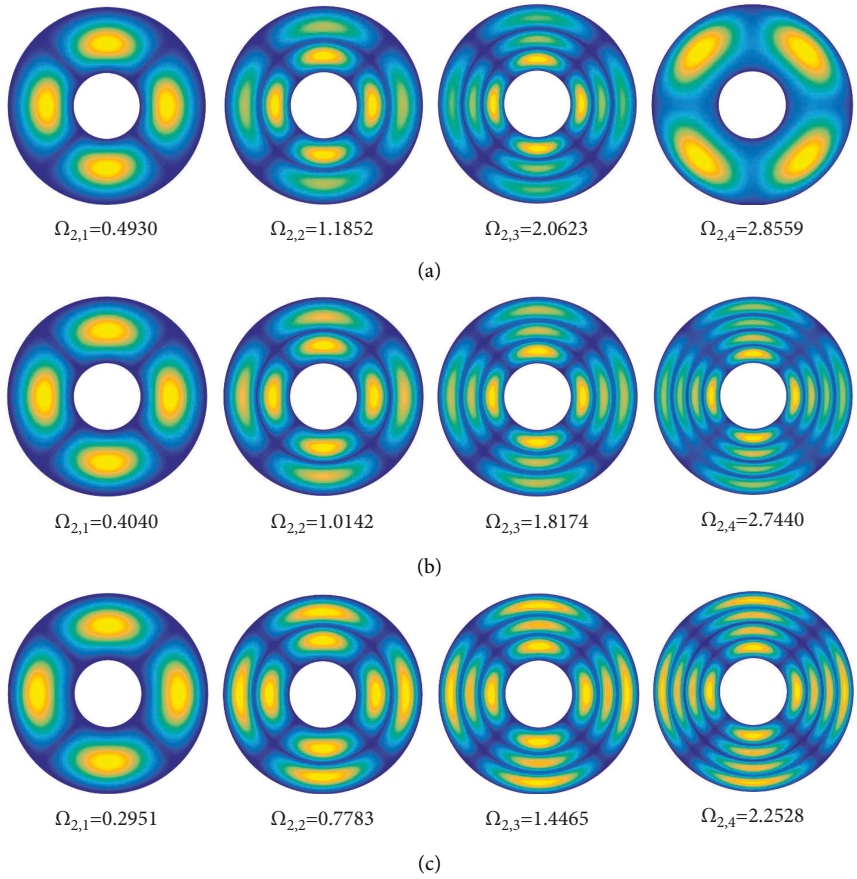


Figure 12: Mode shapes of laminated composite annular plate with variable thickness, (a) $\alpha = -0.5$, (b) $\alpha = 0$, and (c) $\alpha = 0.5$.

geometric dimensions are the same as Figure 8. In here, the parameters for thickness profile $\alpha$ = -0.5, 0 and 0.5, $\lambda = 1$ and material properties and geometric dimensions are the same as Figure 5. The elastic modulus ratios E11/$E22$ vary from 1 to 40. From Figure 9, it is obvious that the frequency parameters increase as the elastic modulus ratios increase.

Some selected mode shapes and their corresponding frequency parameters for the four-layered [0°/90°/0°/90°] laminated composite conical shell, cylindrical shell, and annular plate with variable thickness and C–C boundary condition are presented in Figures 10 and 11, and Figure 12 is helpful in understanding the free vibration characteristics of the laminated composite structures. The material properties are E11/$E22 = 15$, and the geometric dimensions are $R = 1$m, $L = 2$m, $h1 = 0.1$ m in the cylindrical shell, $R1 = 1$m, $L = 2$m, $\varphi = 30°$, $h1 = 0.1$ m in the conical shell, and $R1 = 1$m, $R2 = 3$m, $h1 = 0.1$ m in the annular plate. To consider the mode shape according to the change of thickness, it chooses $\alpha$ = -0.5, 0 and 0.5, $\lambda = 1$. In Figures 10–12, the mode shape of laminated composite structure with varying thickness is different from that of the laminated composite structure with even thickness.

## 4. Conclusion

In this study, a simple and accurate numerical solution method on the basis of the HWDM is presented to study the free vibrational behavior of the laminated composite conical shell, cylindrical shell, and annular plate with variable thickness, in which the thickness of the shell varies linearly or nonlinearly along the longitudinal direction. FSDT is employed for the formulation of theoretical analysis. The displacement and rotation components at any point of structures have expanded the Haar wavelet series in the meridional direction and trigonometric series in the circumferential direction. The results obtained from the current method are compared with those of the previous literature. The results indicated that the proposed method

has high accuracy and reliability in obtaining the frequencies of the laminated composite structures with variable thickness. Also, the effects of several parameters, such as geometrical parameters, thickness variation parameters, different types of boundary conditions, and material properties are investigated. Lastly, new free vibration analysis results are provided for the laminated composite conical shell, cylindrical shell, and annular plate with variable thickness and arbitrary boundary conditions, which can be used as reference results for subsequent pieces of research in this field.

## Appendix

## A. Detailed Expressions of Differential Operator Lij

$$L_{11} = A_{11}\frac{\partial^2}{\partial x^2} + \frac{2A_{16}}{R}\frac{\partial^2}{\partial x\partial\theta} + \frac{A_{66}}{R^2}\frac{\partial^2}{\partial\theta^2} + \frac{A_{11}\sin\varphi}{R}\frac{\partial}{\partial x} - A_{22}\frac{\sin^2\varphi}{R^2} + \frac{\partial A_{11}}{\partial x}\frac{\partial}{\partial x} + \frac{1}{R}\frac{\partial A_{16}}{\partial x}\frac{\partial}{\partial\theta} + \frac{\partial A_{12}}{\partial x}\frac{\sin\varphi}{R}, \tag{A.1}$$

$$L_{12} + \frac{\partial A_{16}}{\partial x}\frac{\partial}{\partial x} + \frac{1}{R}\frac{\partial A_{12}}{\partial x}\frac{\partial}{\partial\theta} - \frac{\partial A_{16}}{\partial x}\frac{\sin\varphi}{R}, \tag{A.2}$$

$$L_{13} = A_{12}\frac{\cos\varphi}{R}\frac{\partial}{\partial x} + A_{26}\frac{\cos\varphi}{R^2}\frac{\partial}{\partial\theta} - A_{22}\frac{\sin\varphi\cos\varphi}{R^2} + \frac{\partial A_{12}}{\partial x}\frac{\cos\varphi}{R}, \tag{A.3}$$

$$L_{14} = B_{11}\frac{\partial^2}{\partial x^2} + \frac{2B_{16}}{R}\frac{\partial^2}{\partial x\partial\theta} + \frac{B_{66}}{R^2}\frac{\partial^2}{\partial\theta^2} + B_{11}\frac{\sin\varphi}{R}\frac{\partial}{\partial x} - B_{22}\frac{\sin^2\varphi}{R^2} + \frac{\partial B_{11}}{\partial x}\frac{\partial}{\partial x} + \frac{1}{R}\frac{\partial B_{16}}{\partial x}\frac{\partial}{\partial\theta} + \frac{\partial B_{12}}{\partial x}\frac{\sin\varphi}{R}, \tag{A.4}$$

$$L_{15} + \frac{\partial B_{16}}{\partial x}\frac{\partial}{\partial x} + \frac{1}{R}\frac{\partial B_{12}}{\partial x}\frac{\partial}{\partial\theta} - \frac{\partial B_{16}}{\partial x}\frac{\sin\varphi}{R}, \tag{A.5}$$

$$L_{21} + \frac{\partial A_{16}}{\partial x}\frac{\partial}{\partial x} + \frac{1}{R}\frac{\partial A_{66}}{\partial x}\frac{\partial}{\partial\theta} + \frac{\partial A_{26}}{\partial x}\frac{\sin\varphi}{R}, \tag{A.6}$$

$$L_{22} = A_{66}\frac{\partial^2}{\partial x^2} + \frac{2A_{26}}{R}\frac{\partial^2}{\partial x\partial\theta} + A_{22}\frac{1}{R^2}\frac{\partial^2}{\partial\theta^2} + A_{66}\frac{\sin\varphi}{R}\frac{\partial}{\partial x} - \left(A_{66}\frac{\sin^2\varphi}{R^2} - \kappa A_{44}\frac{\cos^2\varphi}{R^2}\right) + \frac{\partial A_{26}}{\partial x}\frac{1}{R}\frac{\partial}{\partial\theta} + \frac{\partial A_{66}}{\partial x}\frac{\partial}{\partial x} - \frac{\partial A_{66}}{\partial x}\frac{\sin\varphi}{R}, \tag{A.7}$$

$$L_{23} = \left(A_{26} + \kappa A_{45}\right)\frac{\cos\varphi}{R}\frac{\partial}{\partial x} + \left(A_{22} + \kappa A_{44}\right)\frac{\cos\varphi}{R^2}\frac{\partial}{\partial\theta} + A_{26}\frac{\sin\varphi\cos\varphi}{R^2} + \frac{\partial A_{26}}{\partial x}\frac{\cos\varphi}{R}, \tag{A.8}$$

$$L_{24} + \left(B_{26}\frac{\sin^2\varphi}{R^2} + \kappa A_{45}\frac{\cos\varphi}{R}\right) + \frac{\partial B_{16}}{\partial x}\frac{\partial}{\partial x} + \frac{\partial B_{66}}{\partial x}\frac{1}{R}\frac{\partial}{\partial\theta} + \frac{\partial B_{26}}{\partial x}\frac{\sin\varphi}{R}, \tag{A.9}$$

$$L_{25} + \frac{\partial B_{66}}{\partial x}\frac{\partial}{\partial x} + \frac{\partial B_{26}}{\partial x}\frac{1}{R}\frac{\partial}{\partial\theta} - \frac{\partial B_{66}}{\partial x}\frac{\sin\varphi}{R}, \tag{A.10}$$

$$L_{31} = -A_{12}\frac{\cos\varphi}{R}\frac{\partial}{\partial x} - A_{26}\frac{\cos\varphi}{R^2}\frac{\partial}{\partial\theta} - A_{22}\frac{\sin\varphi\cos\varphi}{R^2}, \tag{A.11}$$

$$L_{32} = -\left(A_{26} + \kappa A_{45}\right)\frac{\cos\varphi}{R}\frac{\partial}{\partial x} - \left(A_{22} + \kappa A_{44}\right)\frac{\cos\varphi}{R^2}\frac{\partial}{\partial\theta} + A_{26}\frac{\sin\varphi\cos\varphi}{R^2} - \kappa\frac{\partial A_{45}}{\partial x}\frac{\cos\varphi}{R}, \tag{A.12}$$

$$L_{33} = \kappa A_{55}\frac{\partial^2}{\partial x^2} + \kappa\frac{2A_{45}}{R}\frac{\partial^2}{\partial x\partial\theta} + \kappa\frac{A_{44}}{R^2}\frac{\partial^2}{\partial\theta^2} + \kappa A_{55}\frac{\sin\varphi}{R}\frac{\partial}{\partial x} - A_{22}\frac{\cos^2\varphi}{R^2} + \kappa\frac{\partial A_{55}}{\partial x}\frac{\partial}{\partial x} + \kappa\frac{1}{R}\frac{\partial A_{45}}{\partial x}\frac{\partial}{\partial\theta}, \tag{A.13}$$

$$L_{34} = \left(\kappa A_{55} - B_{12}\frac{\cos\varphi}{R}\right)\frac{\partial}{\partial x} + \left(\kappa\frac{A_{45}}{R} - B_{26}\frac{\cos\varphi}{R^2}\right)\frac{\partial}{\partial\theta} + \left(\kappa A_{55}\frac{\sin\varphi}{R} - B_{22}\frac{\sin\varphi\cos\varphi}{R^2}\right) + \kappa\frac{\partial A_{55}}{\partial x}, \tag{A.14}$$

$$L_{35} = \left(\kappa A_{45} - B_{26}\frac{\cos\varphi}{R}\right)\frac{\partial}{\partial x} + \left(\kappa\frac{A_{44}}{R} - B_{22}\frac{\cos\varphi}{R^2}\right)\frac{\partial}{\partial\theta} + \left(\kappa A_{45}\frac{\sin\varphi}{R} + B_{26}\frac{\sin\varphi\cos\varphi}{R^2}\right) + \kappa\frac{\partial A_{45}}{\partial x}, \tag{A.15}$$

$$L_{41} = B_{11}\frac{\partial^2}{\partial x^2} + \frac{2B_{16}}{R}\frac{\partial^2}{\partial x\partial\theta} + B_{66}\frac{1}{R^2}\frac{\partial^2}{\partial\theta^2} + B_{11}\frac{\sin\varphi}{R}\frac{\partial}{\partial x} - B_{22}\frac{\sin^2\varphi}{R^2}u + \frac{\partial B_{11}}{\partial x}\frac{\partial}{\partial x} + \frac{1}{R}\frac{\partial B_{16}}{\partial x}\frac{\partial}{\partial\theta} + \frac{\partial B_{12}}{\partial x}\frac{\sin\varphi}{R}, \tag{A.16}$$

$$L_{42} + \left(B_{26}\frac{\sin^2\varphi}{R^2} + \kappa A_{45}\frac{\cos\varphi}{R}\right) + \frac{1}{R}\frac{\partial B_{12}}{\partial x}\frac{\partial}{\partial\theta} + \frac{\partial B_{16}}{\partial x}\frac{\partial}{\partial x} - \frac{\partial B_{16}}{\partial x}\frac{\sin\varphi}{R}, \tag{A.17}$$

$$L_{43} = \left(B_{12}\frac{\cos\varphi}{R} - \kappa A_{55}\right)\frac{\partial}{\partial x} + \left(B_{26}\frac{\cos\varphi}{R^2} - \kappa A_{45}\frac{1}{R}\right)\frac{\partial}{\partial\theta} - B_{22}\frac{\sin\varphi\cos\varphi}{R^2} + \frac{\partial B_{12}}{\partial x}\frac{\cos\varphi}{R}, \tag{A.18}$$

$$L_{44} + \frac{\partial D_{11}}{\partial x}\frac{\partial}{\partial x} + \frac{\partial D_{12}}{\partial x}\frac{\sin\varphi}{R} + \frac{1}{R}\frac{\partial D_{16}}{\partial x}\frac{\partial}{\partial\theta}, \tag{A.19}$$

$$L_{45} + \frac{\partial D_{12}}{\partial x}\frac{1}{R}\frac{\partial}{\partial\theta} + \frac{\partial D_{16}}{\partial x}\frac{\partial}{\partial x} - \frac{\partial D_{16}}{\partial x}\frac{\sin\varphi}{R}, \tag{A.20}$$

$$L_{51} + \frac{\partial B_{16}}{\partial x}\frac{\partial}{\partial x} + \frac{\partial B_{66}}{\partial x}\frac{1}{R}\frac{\partial}{\partial\theta} + \frac{\partial B_{26}}{\partial x}\frac{\sin\varphi}{R}, \tag{A.21}$$

$$L_{52} + \frac{\partial B_{66}}{\partial x}\frac{\partial}{\partial x} + \frac{\partial B_{26}}{\partial x}\frac{1}{R}\frac{\partial}{\partial\theta} - \frac{\partial B_{66}}{\partial x}\frac{\sin\varphi}{R}, \tag{A.22}$$

$$L_{53} = \left(B_{26}\frac{\cos\varphi}{R} - \kappa A_{45}\right)\frac{\partial}{\partial x} + \left(B_{22}\frac{\cos\varphi}{R^2} - \kappa A_{44}\frac{1}{R}\right)\frac{\partial}{\partial\theta} + B_{26}\frac{\sin\varphi\cos\varphi}{R^2} + \frac{\partial B_{26}}{\partial x}\frac{\cos\varphi}{R}, \tag{A.23}$$

$$L_{54} + \left(D_{26}\frac{\sin^2\varphi}{R^2} - \kappa A_{45}\right) + \frac{\partial D_{16}}{\partial x}\frac{\partial}{\partial x} + \frac{1}{R}\frac{\partial D_{66}}{\partial x}\frac{\partial}{\partial\theta} + \frac{\partial D_{26}}{\partial x}\frac{\sin\varphi}{R}, \tag{A.24}$$

$$L_{55} + \frac{\partial D_{26}}{\partial x}\frac{1}{R}\frac{\partial}{\partial\theta} + \frac{\partial D_{66}}{\partial x}\frac{\partial}{\partial x} - \frac{\partial D_{66}}{\partial x}\frac{\sin\varphi}{R}.$$

## B. Detailed Expressions of the Constant Coefficients Lijk

$L_{11}^0$

$$L_{12}^0 = -A_{22}n\sin\varphi - A_{66}n\sin\varphi + \frac{\partial A_{12}}{\partial x}nR, L_{12}^1 = (A_{12} + A_{66})nR,$$

$$L_{13}^0 = -A_{22}\sin\varphi\cos\varphi + \frac{\partial A_{12}}{\partial x}R\cos\varphi, L_{13}^1 = A_{12}\cos\varphi, \tag{A.26}$$

$$L_{14}^0 = -B_{22}\sin^2\varphi - B_{66}n^2 + \frac{\partial B_{12}}{\partial x}R\sin\varphi, L_{14}^1 = B_{11}R\sin\varphi + \frac{\partial B_{11}}{\partial x}R^2, L_{14}^2 = B_{11}R^2,$$

$$L_{15}^0 = -B_{22}n\sin\varphi - B_{66}n\sin\varphi + \frac{\partial B_{12}}{\partial x}R^2, L_{15}^1 = (B_{12} + B_{66})nR.$$

$L_{21}^0$

$$\begin{aligned}
&L_{22}^0 = -A_{66}\sin^2\varphi - A_{22}n^2 - \frac{\partial A_{66}}{\partial x}R\sin\varphi - \kappa A_{44}\cos^2\varphi, L_{22}^1 = A_{66}R\sin\varphi + \frac{\partial A_{66}}{\partial x}R^2, L_{22}^2 = A_{66}R^2,\\
&L_{23}^0 = -(A_{22} + \kappa A_{44})n\cos\varphi,\\
&L_{24}^0 = -B_{22}n\sin\varphi - B_{66}n\sin\varphi - \frac{\partial B_{66}}{\partial x}nR, L_{24}^1 = -(B_{12} + B_{66})nR,\\
&L_{25}^0 = -B_{66}\sin^2\varphi - B_{22}n^2 - \frac{\partial B_{66}}{\partial x}R\sin\varphi + \kappa A_{44}R\cos\varphi, L_{25}^1 = B_{66}R\sin\varphi + \frac{\partial B_{66}}{\partial x}R^2, L_{25}^2 = B_{66}R^2,
\end{aligned} \tag{A.27}$$

$L_{31}^0$

$$\begin{aligned}
&L_{33}^0 = -\kappa A_{44}n^2 - A_{22}\cos^2\varphi, L_{33}^1 = \kappa A_{55}R\sin\varphi + \kappa\frac{\partial A_{55}}{\partial x}R^2, L_{33}^2 = \kappa A_{55}R^2,\\
&L_{34}^0 = \kappa A_{55}R\sin\varphi - B_{22}\sin\varphi\cos\varphi + \kappa\frac{\partial A_{55}}{\partial x}R^2, L_{34}^1 = \kappa A_{55}R^2 - B_{12}R\cos\varphi,\\
&L_{35}^0 = (\kappa A_{44}R - B_{22}\cos\varphi)n,
\end{aligned} \tag{A.28}$$

$L_{41}^0$

$$\begin{aligned}
&L_{42}^0 = -B_{22}n\sin\varphi - B_{66}n\sin\varphi + \frac{\partial B_{12}}{\partial x}nR, L_{42}^1 = (B_{12} + B_{66})nR,\\
&L_{43}^0 = -B_{22}\sin\varphi\cos\varphi + \frac{\partial B_{12}}{\partial x}R\cos\varphi, L_{43}^1 = B_{12}R\cos\varphi - \kappa A_{55}R^2,\\
&L_{44}^0 = -D_{22}\sin^2\varphi - D_{66}n^2 - \kappa A_{55} + \frac{\partial D_{12}}{\partial x}R\sin\varphi, L_{44}^1 = D_{11}R\sin\varphi + \frac{\partial D_{11}}{\partial x}R^2, L_{44}^2 = D_{11}R^2,\\
&L_{45}^0 = -D_{22}n\sin\varphi - D_{66}n\sin\varphi - \frac{\partial D_{12}}{\partial x}nR, L_{45}^1 = (D_{12} + D_{66})nR,
\end{aligned} \tag{A.29}$$

$L_{51}^0$

$$\begin{aligned}
&L_{52}^0 = \kappa A_{44}R\cos\varphi - B_{22}n^2 - B_{66}\sin^2\varphi - \frac{\partial B_{66}}{\partial x}R\sin\varphi, L_{52}^1 = B_{66}R\sin\varphi + \frac{\partial B_{66}}{\partial x}R^2, L_{52}^2 = B_{66}R^2,\\
&L_{53}^0 = -(B_{22}\cos\varphi - \kappa A_{44}R)n,\\
&L_{54}^0 = -n\sin\varphi D_{22} - n\sin\varphi D_{66} - \frac{\partial D_{66}}{\partial x}nR, L_{54}^1 = -(D_{12} + D_{66})nR,\\
&L_{55}^0 = -D_{66}\sin^2\varphi - D_{22}n^2 - \frac{\partial D_{66}}{\partial x}R\sin\varphi - \kappa A_{44}R^2, L_{55}^1 = D_{66}R\sin\varphi + \frac{\partial D_{66}}{\partial x}R^2, L_{55}^2 = D_{66}R^2.
\end{aligned} \tag{A.30}$$

## Data Availability

All data that support the findings of this study are included within the article.

## Conflicts of Interest

The authors declare that they have no conflicts of interest.

## Acknowledgments

The authors would like to take the opportunity to express their hearty gratitude to all those who made a contribution to the completion of this article. In addition, the authors would like to thank the authors of "Free vibration analysis of laminated composite conical cylindrical shell and annular plate with variable thickness and general boundary conditions" for their assistance in this study.

## References

[1] A. A. Khdeir, J. N. Reddy, and D. Frederick, "A study of bending, vibration and buckling of cross-ply circular cylindrical shells with various shell theories," *International Journal of Engineering Science*, vol. 27, no. 11, pp. 1337–1351, 1989.

[2] T. Ich Thinh and M. C. Nguyen, "Dynamic stiffness matrix of continuous element for vibration of thick cross-ply laminated composite cylindrical shells," *Composite Structures*, vol. 98, pp. 93–102, 2013.

[3] G. Jin, T. Ye, X. Ma, Y. Chen, Z. Su, and X. Xie, "A unified approach for the vibration analysis of moderately thick composite laminated cylindrical shells with arbitrary boundary conditions," *International Journal of Mechanical Sciences*, vol. 75, pp. 357–376, 2013.

[4] X. Xie, G. Jin, and Z. Liu, "Free vibration analysis of cylindrical shells using the Haar wavelet method," *International Journal of Mechanical Sciences*, vol. 77, pp. 47–56, 2013.

[5] X. Xie, G. Jin, Y. Yan, S. X. Shi, and Z. Liu, "Free vibration analysis of composite laminated cylindrical shells using the Haar wavelet method," *Composite Structures*, vol. 109, pp. 169–177, 2014.

[6] G. Jin, X. Xie, and Z. Liu, "The Haar wavelet method for free vibration analysis of functionally graded cylindrical shells based on the shear deformation theory," *Composite Structures*, vol. 108, pp. 435–448, 2014.

[7] Y. Qu, X. Long, S. Wu, and G. Meng, "A unified formulation for vibration analysis of composite laminated shells of revolution including shear deformation and rotary inertia," *Composite Structures*, vol. 98, pp. 169–191, 2013.

[8] D. He, D. Shi, Q. Wang, and C. Ma, "A unified power series method for vibration analysis of composite laminate conical, cylindrical shell and annular plate," *Structures*, vol. 29, pp. 305–327, 2021.

[9] X. Xiang, J. Guoyong, L. Wanyou, and L. Zhigang, "A numerical solution for vibration analysis of composite laminated conical, cylindrical shell and annular plate structures," *Composite Structures*, vol. 111, pp. 20–30, 2014.

[10] G. Jin, T. Ye, X. Jia, and S. Gao, "A general Fourier solution for the vibration analysis of composite laminated structure elements of revolution with general elastic restraints," *Composite Structures*, vol. 109, pp. 150–168, 2014.

[11] X. Xie, G. Jin, T. Ye, and Z. Liu, "Free vibration analysis of functionally graded conical shells and annular plates using the Haar wavelet method," *Applied Acoustics*, vol. 85, pp. 130–142, 2014.

[12] A. H. Yousefi, P. Memarzadeh, H. Afshari, and S. J. Hosseini, "Agglomeration effects on free vibration characteristics of three-phase CNT/polymer/fiber laminated truncated conical shells," *Thin-Walled Structures*, vol. 157, Article ID 107077, 2020.

[13] H. Afshari and H. Amirabadi, "Vibration characteristics of rotating truncated conical shells reinforced with agglomerated carbon nanotubes," *Journal of Vibration and Control*, vol. 28, no. 15-16, pp. 1894–1914, 2021.

[14] H. Afshari, "Free vibration analysis of GNP-reinforced truncated conical shells with different boundary conditions," *Australian Journal of Mechanical Engineering*, pp. 1–17, 2020.

[15] H. Afshari, "Effect of graphene nanoplatelet reinforcements on the dynamics of rotating truncated conical shells," *Journal of the Brazilian Society of Mechanical Sciences and Engineering*, vol. 42, no. 10, 519 pages, 2020.

[16] N. Adab, M. Arefi, and M. Amabili, "A comprehensive vibration analysis of rotating truncated sandwich conical microshells including porous core and GPL-reinforced facesheets," *Composite Structures*, vol. 279, Article ID 114761, 2022.

[17] N. Adab and M. Arefi, "Vibrational behavior of truncated conical porous GPL-reinforced sandwich micro/nano-shells," *Engineering with Computers*, 2022.

[18] H. Afshari, Y. Ariaseresht, S. S. R. Koloor, H. Amirabadi, and M. Omidi Bidgoli, "Supersonic flutter behavior of a polymeric truncated conical shell reinforced with agglomerated CNTs," *Waves in Random and Complex Media*, vol. 32, 2022.

[19] A. H. Yousefi, P. Memarzadeh, H. Afshari, and S. J. Hosseini, "Optimization of CNT/polymer/fiber laminated truncated conical panels for maximum fundamental frequency and minimum cost," *Mechanics Based Design of Structures and Machines*, pp. 1–23, 2021.

[20] A. H. Yousefi, P. Memarzadeh, H. Afshari, and S. Jalil Hosseini, "Dynamic characteristics of truncated conical panels made of FRPs reinforced with agglomerated CNTs," *Structures*, vol. 33, pp. 4701–4717, 2021.

[21] T. Irie, G. Yamada, and Y. Kaneko, "Free vibration of a conical shell with variable thickness," *Journal of Sound and Vibration*, vol. 82, no. 1, pp. 83–94, 1982.

[22] K. R. Sivadas and N. Ganesan, "Free vibration of cantilever conical shells with variable thickness," *Computers & Structures*, vol. 36, no. 3, pp. 559–566, 1990.

[23] N. Ganesan and K. R. Sivadas, "Vibration analysis of orthotropic shells with variable thickness," *Computers & Structures*, vol. 35, no. 3, pp. 239–248, 1990.

[24] K. R. Sivadas and N. Ganesan, "Axisymmetric vibration analysis of thick cylindrical shell with variable thickness," *Journal of Sound and Vibration*, vol. 160, no. 3, pp. 387–400, 1993.

[25] K. R. Sivadas and N. Ganesan, "Asymmetric vibration analysis of thick composite circular cylindrical shells with variable thickness," *Computers & Structures*, vol. 38, no. 5-6, pp. 627–635, 1991.

[26] K. R. Sivadas and N. Ganesan, "Vibration analysis of laminated conical shells with variable thickness," *Journal of Sound and Vibration*, vol. 148, no. 3, pp. 477–491, 1991.

[27] B. P. Gautham and N. Ganesan, "Axisymmetric vibration of layered orthotropic spherical shells of variable thickness," *Computers & Structures*, vol. 45, no. 5-6, pp. 893–900, 1992.

[28] N. Sankaranarayanan, K. Chandrasekaran, and G. Ramaiyan, "Axisymmetric vibrations of laminated conical shells of variable thickness," *Journal of Sound and Vibration*, vol. 118, no. 1, pp. 151–161, 1987.

[29] N. Sankaranarayanan, K. Chandrasekaran, and G. Ramaiyan, "Free vibrations of laminated conical shells of variable thickness," *Journal of Sound and Vibration*, vol. 123, no. 2, pp. 357–371, 1988.

[30] W. Jiang and D. Redekop, "Static and vibration analysis of orthotropic toroidal shells of variable thickness by differential

quadrature," *Thin-Walled Structures*, vol. 41, no. 5, pp. 461–478, 2003.

[31] W. Duan and C. G. Koh, "Axisymmetric transverse vibrations of circular cylindrical shells with variable thickness," *Journal of Sound and Vibration*, vol. 317, no. 3-5, pp. 1035–1041, 2008.

[32] Z. Chen, L. Yang, G. Cao, and W. Guo, "Buckling of the axially compressed cylindrical shells with arbitrary axisymmetric thickness variation," *Thin-Walled Structures*, vol. 60, pp. 38–45, 2012.

[33] M. Liu, J. Liu, and Y. Cheng, "Free vibration of a fluid loaded ring-stiffened conical shell with variable thickness," *Journal of Vibration and Acoustics*, vol. 136, no. 5, pp. 1–10, 2014.

[34] T. H. Quoc, D. T. Huan, and H. T. Phuong, "Vibration characteristics of rotating functionally graded circular cylindrical shell with variable thickness under thermal environment," *International Journal of Pressure Vessels and Piping*, vol. 193, Article ID 104452, 2021.

[35] N. El-Kaabazi and D. Kennedy, "Calculation of natural frequencies and vibration modes of variable thickness cylindrical shells using the Wittrick-Williams algorithm," *Computers & Structures*, vol. 104-105, pp. 4–12, 2012.

[36] S. Afonso and E. Hinton, "Free vibration analysis and shape optimization of variable thickness plates and shells-I. Finite element studies," *Computing Systems in Engineering*, vol. 6, no. 1, pp. 27–45, 1995.

[37] S. Afonso and E. Hinton, "Free vibration analysis and shape optimization of variable thickness plates and shells-II. Sensitivity analysis and shape optimization," *Computing Systems in Engineering*, vol. 6, no. 1, pp. 47–66, 1995.

[38] E. Taati, F. Fallah, and M. T. Ahmadian, "Closed-form solution for free vibration of variable-thickness cylindrical shells rotating with a constant angular velocity," *Thin-Walled Structures*, vol. 166, Article ID 108062, 2021.

[39] E. Efraim and M. Eisenberger, "Dynamic stiffness vibration analysis of thick spherical shell segments with variable thickness," *Journal of Mechanics of Materials and Structures*, vol. 5, pp. 821–835, 2010.

[40] D. Zheng, J. Du, and Y. Liu, "Vibration characteristics analysis of an elastically restrained cylindrical shell with arbitrary thickness variation," *Thin-Walled Structures*, vol. 165, Article ID 107930, 2021.

[41] F. Tornabene, N. Fantuzzi, and M. Bacciocchi, "The local GDQ method for the natural frequencies of doubly-curved shells with variable thickness: a general formulation," *Composites Part B: Engineering*, vol. 92, pp. 265–289, 2016.

[42] F. Tornabene, M. Viscoti, R. Dimitri, and J. N. Reddy, "Higher order theories for the vibration study of doubly-curved anisotropic shells with a variable thickness and isogeometric mapped geometry," *Composite Structures*, vol. 267, Article ID 113829, 2021.

[43] M. Bacciocchi, M. Eisenberger, N. Fantuzzi, F. Tornabene, and E. Viola, "Vibration analysis of variable thickness plates and shells by the Generalized Differential Quadrature method," *Composite Structures*, vol. 156, pp. 218–237, 2016.

[44] F. Tornabene, N. Fantuzzi, M. Bacciocchi, and E. Viola, "Accurate inter-laminar recovery for plates and doubly-curved shells with variable radii of curvature using layer-wise theories," *Composite Structures*, vol. 124, pp. 368–393, 2015.

[45] F. Tornabene, N. Fantuzzi, M. Bacciocchi, and E. Viola, "A new approach for treating concentrated loads in doubly-curved composite deep shells with variable radii of curvature," *Composite Structures*, vol. 131, pp. 433–452, 2015.

[46] F. Tornabene, N. Francesco, and E. Viola, "Inter-laminar stress recovery procedure for doubly-curved, singly-curved, revolution shells with variable radii of curvature and plates using generalized higher-order theories and the local GDQ method," *Mechanics of Advanced Materials and Structures*, vol. 23, no. 9, pp. 1019–1045, 2016.

[47] J.-H. Kang and A. W. Leissa, "Three-dimensional vibrations of thick spherical shell segments with variable thickness," *International Journal of Solids and Structures*, vol. 37, no. 35, pp. 4811–4823, 2000.

[48] J.-H. Kang and A. W. Leissa, "Free vibration analysis of complete paraboloidal shells of revolution with variable thickness and solid paraboloids from a three-dimensional theory," *Computers & Structures*, vol. 83, no. 31-32, pp. 2594–2608, 2005.

[49] A. W. Leissa and J. H. Kang, "Three-dimensional vibration analysis of paraboloidal shells," *JSME International Journal Series C*, vol. 45, no. 1, pp. 2–7, 2002.

[50] J.-H. Kang and A. W. Leissa, "Corrigendum to "Three-dimensional vibrations of thick spherical shell segments with variable thickness" [International Journal of Solids and Structures 37 (2000) 4811–4823]," *International Journal of Solids and Structures*, vol. 43, no. 9, pp. 2848–2851, 2006.

[51] J.-H. Kang and A. W. Leissa, "Three-Dimensional vibration analysis of solid and hollow hemispheres having varying thicknesses with and without axial conical holes," *Journal of Vibration and Control*, vol. 10, no. 2, pp. 199–214, 2004.

[52] J.-H. Kang and A. W. Leissa, "Three-dimensional field equations of motion, and energy functionals for thick shells of revolution with arbitrary curvature and variable thickness," *Journal of Applied Mechanics*, vol. 68, no. 6, pp. 953-954, 2001.

[53] J.-H. Kang, "Three-dimensional vibration analysis of joined thick conical — cylindrical shells of revolution with variable thickness," *Journal of Sound and Vibration*, vol. 331, no. 18, pp. 4187–4198, 2012.

[54] Y.-B. Yang and J.-H. Kang, "Vibrations of a composite shell of hemiellisoidal-cylindrical shell having variable thickness with and without a top opening," *Thin-Walled Structures*, vol. 119, pp. 677–686, 2017.

[55] C. F. Chen and C. H. Hsiao, "Haar wavelet method for solving lumped and distributed parameter systems," *IEE Proceedings - Control Theory and Applications*, vol. 144, no. 1, pp. 87–94, 1997.

[56] C. H. Hsiao, "State analysis of linear time-delayed systems via Haar wavelets," *Mathematics and Computers in Simulation*, vol. 44, no. 5, pp. 457–470, 1997.

[57] C. H. Hsiao and W. J. Wang, "Haar wavelet approach to nonlinear stiff systems," *Mathematics and Computers in Simulation*, vol. 57, no. 6, pp. 347–353, 2001.

[58] Ü. Lepik, "Numerical solution of differential equations using Haar wavelets," *Mathematics and Computers in Simulation*, vol. 68, no. 2, pp. 127–143, 2005.

[59] Ü. Lepik, "Solving PDEs with the aid of two-dimensional Haar wavelets," *Computers & Mathematics with Applications*, vol. 61, no. 7, pp. 1873–1879, 2011.

[60] Z. Shi and Y. Y. Cao, "A spectral collocation method based on Haar wavelets for Poisson equations and biharmonic equations," *Mathematical and Computer Modelling*, vol. 54, no. 11-12, pp. 2858–2868, 2011.

[61] Z. Shi and Y. Y. Cao, "Application of Haar wavelet method to eigenvalue problems of high order differential equations," *Applied Mathematical Modelling*, vol. 36, no. 9, pp. 4020–4026, 2012.

[62] N. M. Bujurke, C. S. Salimath, and S. C. Shiralashetti, "Computation of eigenvalues and solutions of regular Sturm–Liouville problems using Haar wavelets," *Journal of*

*Computational and Applied Mathematics*, vol. 219, no. 1, pp. 90–101, 2008.

[63] J. Majak, M. Pohlak, M. Eerme, and T. Lepikult, "Weak formulation based Haar wavelet method for solving differential equations," *Applied Mathematics and Computation*, vol. 211, no. 2, pp. 488–494, 2009.

[64] M. Kirs, M. Mikola, A. Haavajõe, E. Õunapuu, B. Shvartsman, and J. Majak, "Haar wavelet method for vibration analysis of nanobeams," *Waves, Wavelets and Fractals*, vol. 2, no. 1, pp. 20–28, 2016.

[65] H. Hein and L. Feklistova, "Free vibrations of non-uniform and axially functionally graded beams using Haar wavelets," *Engineering Structures*, vol. 33, no. 12, pp. 3696–3701, 2011.

[66] H. Hein and L. Feklistova, "Computationally efficient delamination detection in composite beams using Haar wavelets," *Mechanical Systems and Signal Processing*, vol. 25, no. 6, pp. 2257–2270, 2011.

[67] G. Kim, P. Han, K. An, D. Choe, Y. Ri, and H. Ri, "Free vibration analysis of functionally graded double-beam system using Haar wavelet discretization method," *Engineering Science and Technology, an International Journal*, vol. 24, no. 2, pp. 414–427, 2021.

[68] K. Kim, P. Han, K. Jong, C. Jang, and R. Kim, "Natural frequency calculation of elastically connected double-beam system with arbitrary boundary condition," *AIP Advances*, vol. 10, no. 5, Article ID 055026, 2020.

[69] C. Zhang and Z. Zhong, "Three-dimensional analysis of functionally graded plate based on the Haar wavelet method," *Acta Mechanica Solida Sinica*, vol. 20, no. 2, pp. 95–102, 2007.

[70] B. H. Kim, H. Kim, and T. Park, "Nondestructive damage evaluation of plates using the multi-resolution analysis of two-dimensional Haar wavelet," *Journal of Sound and Vibration*, vol. 292, no. 1-2, pp. 82–104, 2006.

[71] X. Xie, H. Zheng, and G. Jin, "Free vibration of four-parameter functionally graded spherical and parabolic shells of revolution with arbitrary boundary conditions," *Composites Part B: Engineering*, vol. 77, pp. 59–73, 2015.

[72] K. Kim, S. Kwak, K. Choe, W. Han, Y. Ri, and K. Ri, "Application of Haar wavelet method for free vibration of laminated composite conical–cylindrical coupled shells with elastic boundary condition," *Physica Scripta*, vol. 96, no. 3, Article ID 035223, 2021.

[73] K. Kim, C. Kim, K. An, S. Kwak, K. Ri, and K. Ri, "Application of Haar wavelet discretization method for free vibration analysis of inversely coupled composite laminated shells," *International Journal of Mechanical Sciences*, vol. 204, Article ID 106549, 2021.

[74] K. An, Y. Jon, K. Kim, S. Kim, and C. Kim, "A solution method for free vibrration analysis of the elastically joined functionally graded shells," *Eur. Phys. J. Plus*, vol. 136, no. 7, pp. 767–832, 2021.

[75] R. Talebitooti and V. S. Anbardan, "Haar wavelet discretization approach for frequency analysis of the functionally graded generally doubly-curved shells of revolution," *Applied Mathematical Modelling*, vol. 67, pp. 645–675, 2019.